Astronomy & Astrophysics manuscript no.
(will be inserted by hand later)

arXiv:astro-ph/0104151v1 9 Apr 2001

A spectrophotometric atlas of Narrow-Line Seyfert 1 galaxies

M.-P. Véron-Cetty[1], P. Véron[1] and A.C. Gonçalves[2]

[1] Observatoire de Haute Provence, CNRS, F-04870 Saint-Michel l'Observatoire, France
e-mail: mira@obs-hp.fr; veron@obs-hp.fr
[2] European Southern Observatory (ESO), Karl Schwarzschild Strasse 2, D-85748 Garching bei München, Germany
e-mail: adarbon@eso.org

Received ; accepted

Abstract. We have compiled a list of 83 objects classified as Narrow-Line Seyfert 1 galaxies (NLS1s) or known to have a broad Balmer component narrower than 2 000 km s^{-1}. Out of these, 19 turned out to have been spectroscopically misidentified in previous studies; only 64 of the selected objects are genuine NLS1s. We have spectroscopically observed 59 of them and tried to characterize their Narrow and Broad-Line Regions (NLR and BLR) by fitting the emission-lines with Gaussian and/or Lorentzian profiles.
In most cases, the broad Balmer components are well fitted by a single Lorentzian profile, confirming previous claims that Lorentzian rather than Gaussian profiles are better suited to reproduce the shape of the NLS1s broad emission lines. This has consequences concerning their FWHMs and line ratios: when the broad Balmer components are fitted with a Lorentzian, most narrow line regions have line ratios typical of Seyfert 2s while, when a Gaussian profile is used for fitting the broad Balmer components, the line ratios are widely scattered in the usual diagnostic diagrams (Veilleux & Osterbrock 1987); moreover, the FWHM of the best fitting Lorentzian is systematically smaller than the FWHM of the Gaussian.
We find that, in general, the [O III] lines have a relatively narrow Gaussian profile ($\sim$ 200–500 km s^{-1} FWHM) with often, in addition, a second broad ($\sim$ 500–1 800 km s^{-1} FWHM), blueshifted Gaussian component. We do not confirm that the [O III] lines are weak in NLS1s.
As previously suggested, there is a continuous transition of all properties between NLS1s and classical Broad-Line Seyfert 1 Galaxies (BLS1s) and the limit of 2 000 km s^{-1} used to separate the two species is arbitrary; R_{4570}, the ratio of the Fe II to the Hβ fluxes, could be a physically more meaningful parameter to distinguish them.

Key words. Galaxies – Seyfert

1. Introduction

Osterbrock & Pogge (1985) have identified a class of AGNs having all properties of the Seyfert 1s with, however, very narrow Balmer lines and strong optical Fe II lines; they are called NLS1s. Quantitatively, a Seyfert 1 is called an NLS1 if the "broad" component of the Balmer lines is narrower than 2 000 km s^{-1} FWHM (Osterbrock 1987). NLS1s often have strong Fe II emission; many of them have a strong soft X-ray excess and display high-amplitude X-ray variability.

The 2–10 keV spectrum of classical BLS1s can be fitted with a power-law with a photon index Γ=1.73±0.05 (Nandra & Pounds 1994; Reynolds 1997; George et al. 1998a); in NLS1s, Γ is significantly steeper (Γ=2.19 ±0.10) (Leighly 1999b); in fact, it is anticorrelated with the Hβ FWHM (Brandt et al. 1997; Reeves & Turner 2000).

Some Seyfert 1s show evidence for an excess of soft X-rays above the hard X-ray power-law extrapolation, dominant below ∼1 keV (Saxton et al. 1993; George et al. 2000). This excess is more important and more frequent in NLS1s than in BLS1s (Vaughan et al. 1999a; Leighly 1999b; Reeves & Turner 2000). The soft photon spectral index Γ (0.1–2.4 keV), which measures the relative strength of the soft component, is correlated with the Balmer line width in the sense that steep soft X-ray spectra corresponds to narrow Balmer lines (Puchnarewicz et al. 1992; Boller et al. 1996; Wang et al. 1996; Laor et al. 1997a). In fact NLS1s may show both steep as well as flat X-ray spectra, while BLS1s always have flat spectra (Grupe et al. 1999). However, several NLS1s show a significant intrinsic neutral hydrogen column density in excess of the Galactic value; the unability to detect a soft excess in the X-ray spectrum of some NLS1s could be due to the presence of such a high column density. Therefore the soft excess may be more prevalent in NLS1s than observed (Leighly 1999b).

Send offprint requests to: P. Véron

Most AGN spectra show the presence of a "Big Blue Bump" (BBB) extending from optical frequencies upwards (Elvis et al. 1986; Sanders et al. 1989). The BBB has been interpreted as the thermal emission of a physically thin, optically thick accretion disk (Sun & Malkan 1989; Siemiginowska et al. 1995). The soft X-ray spectral index is correlated to the strength of the ultraviolet bump in unabsorbed Seyfert 1s, indicating that the BBB is in fact an ultraviolet to soft X-ray bump (Walter & Fink 1993; Puchnarewicz et al. 1995; Page et al. 1999). NLS1s have significantly bluer spectra than BLS1s which is consistent with the presence of a more pronounced BBB in NLS1s (Grupe et al. 1998). However, when sufficient data are available, it seems that a single standard accretion disk model cannot fit the optical/UV/X-ray bump (Kolman et al. 1993; Wisotzki et al. 1995).

NLS1s very frequently exhibit rapid and/or high-amplitude X-ray variability (Boller et al. 1996; Forster & Halpern 1996; Molthagen et al. 1998). The X-ray-steep, narrow-Hβ AGNs systematically show larger amplitude variations than the X-ray-flat, broad-Hβ AGNs on time scales from 2 to 20 days (Fiore et al. 1998; Leighly 1999a; Turner et al. 1999b). Observed variability by a factor 2 in a few hours or less shows that a substantial fraction of the soft component comes from a compact region, smaller than a light-day. Giant-amplitude X-ray variability (from one up to more than two orders of magnitude on a time scale of one to a few years) has been observed in several NLS1s (see for instance Brandt et al. 1999 and Uttley et al. 1999). In the cases of NGC 4051 and IRAS 13224−3809, changes by a factor of 10 or more have occured within a few hours (Leighly 1999a). It is quite remarkable that all these objects, except NGC 4051, have a very high soft photon index ($\Gamma > 4$), at least when they are bright.

A few BLS1s have also displayed X-ray flux variability by a factor of 10 or more such as NGC 3227 ($\times$15) (Komossa & Fink 1997a; George et al. 1998b) and NGC 3786 ($\times$10) (Komossa & Fink 1997b); in both cases, however, the variability has been attributed to a change in the column density of a warm absorber.

A number of observations suggests that NLS1s are Seyfert 1s with a near- or super-Eddington accretion rate.

If the broad-line emitting region is gravitationally linked to the central black hole (BH), one can show that the FWHM of the lines depends on the mass of the BH, the ratio of the luminosity to the Eddington luminosity and the angle between the rotation axis of the gas disk and the line of sight. The NLS1s could be either normal Seyfert 1s seen perpendicularly to the disk, or objects with a low mass BH radiating near the Eddington limit (Wang et al. 1996).

The combination of strong soft X-ray excess and steep power law prompted Pounds et al. (1995) to postulate that NLS1s represent the supermassive BH analogue of Galactic BH candidates (GBHC) in their high states. The high states of GBHCs are thought to be triggered by increases in the accretion rate resulting in strong thermal emission from a disk accreting at the Eddington limit.

Standard accretion disks are not able to account for the soft X-ray excess unless the Eddington ratio is close to unity; a large accretion rate results in a more pronouced BBB which is shifted toward higher energies, resulting in stronger soft X-ray emission and hence steeper soft X-ray slope (Pounds et al. 1987; Ross et al. 1992; Kuraszkiewicz et al. 2000).

At a fixed luminosity, BHs radiating at higher fractions of the Eddington rate will have lower masses; lower mass BHs are thought to be associated with physically smaller emission regions that vary more rapidly. This may explain why higher amplitude short term X-ray variability is observed in NLS1s (Fiore et al. 1998; Leighly 1999a; Turner et al. 1999b).

Nicastro (2000) proposed a model in which, for accretion rates $\dot{M}/\dot{M}_{\rm Edd} < 0.2$ (sub-Eddington regime), the predicted FWHMs are quite broad (>4 000 km s^{-1}), while for $\dot{M}/\dot{M}_{\rm Edd}$=0.2-3 (Eddington to moderately super-Eddington), the corresponding FWHMs span the interval $\approx$1 000-4 000 km s^{-1}.

The amount of published data on NLS1s increased dramatically over the last few years, specially since the launch of the *ROSAT* and *ASCA* satellites, and important progresses have been made in the X-ray domain. NLS1s however are still subject to much debate; our knowledge of the basic properties concerning their emission-line regions (line profiles, line ratios, etc.), and of their relation to the X-ray properties, is still rather limited, as is the relationship between NLS1s and classical BLS1s. This is largely due to the fact that little effort has been put in providing a set of high-quality optical spectroscopic data. Published data are very heterogeneous; spectra often have a resolution insufficient to separate unambiguously the broad and narrow components of the Balmer lines; in addition, the presence of strong Fe II lines makes it difficult to measure Hβ.

Aware of the fact that a detailed and consistent study of NLS1 emission-line properties was missing and that the knowledge of these properties is of crucial importance for understanding the basic physical differences between BLS1s and NLS1s and, ultimately, for fitting them into the standard unifying picture, we have obtained a homogeneous set of moderate resolution (3.4 Å FWHM or 200 km s^{-1} at Hβ) spectra around Hα and/or Hβ of a large number of NLS1s; this setting turned out to be adequate as narrow line individual components are, in most cases, resolved with this resolution; however, in the few objects where a H II region is present near the galaxy nucleus a better resolution would of course allow to separate more easily the Seyfert 2 emission lines from the much narrower H II lines.

2. Observations and data reduction

We have compiled all 83 objects known to us before January 1998 either to be NLS1s or to have a "broad" Balmer component narrower than 2 000 km s^{-1}, north of $\delta = -25^{o}$, brighter than B=17.0 and with z < 0.100. We have spectroscopically observed 76 of them.

Table 1. Observations dates and standard stars

Date	λ range (Å)	Standard stars
21.03.95	6500 – 7400	BD 26°2606
31.08.95	4855 – 5755	Feige 15, BD 25°3941
01.09.95	4855 – 5755	and BD 28°4211
10.05.96	6700 – 7600	GD 140, BD 26°2606
11.05.96	4860 – 5760	Feige 98, Kopff 27
15 – 16.07.96	4675 – 5575	BD 28°4211
24.07.96	6335 – 7235	BD 28°4211
07.01.97	4720 – 5620	EG 247
09 – 10.01.97	6175 – 7075	EG 247
04 – 07.03.97	4825 – 5725	Feige 66
08 – 12.03.97	6310 – 7210	Feige 66
13.03.97	4825 – 5725	Feige 66
29.10.97	6500 – 6950	Feige 24, EG 247
30.10.97	4825 – 5280	Feige 24, EG 247
31.10.97	6455 – 7355	Feige 24
01 – 02.11.97	4655 – 5555	Feige 24
27 – 29.05.98	4645 – 5545	Feige 66, Kopff 27
31.05.98	6430 – 7330	Feige 66
15.06.98	4420 – 6265	GD 190
16.06.98	6020 – 7870	GD 190
23.09.00	4255 – 6090	Feige 15, EG 247

– On October 29 and 30, 1997, we have used a dispersion of 33 Å mm^{-1} instead of 66 Å mm^{-1}.
– In June 1998 and September 2000, we have used an EEV 42-20 instead of a TK 512 CCD

The observations were carried out during several observing runs with the spectrograph CARELEC (Lemaître et al. 1989) attached to the Cassegrain focus of the Observatoire de Haute-Provence (OHP) 1.93 m telescope. Table 1 gives the list of observing runs with the observed wavelength ranges and the standard stars used.

The detector was a 512×512 pixels, 27×27 μm Tektronic CCD, except in June 1998 and September 2000 when we used a 1024×2048 pixels, 13.5×13.5 μm EEV 42-20 CCD. We generally used a 600 l mm^{-1} grating resulting in a dispersion of 66 Å mm^{-1}. On October 29 and 30, 1997, we used a dispersion of 33 Å mm^{-1}. In each case, the galaxy nucleus was centered on the slit. Three to five columns of the CCD (3 to 5″) were extracted on the Tektronic CCD and 7 column (∼3″) on the EEV. The slit width was 2.″1, corresponding to a projected slit width on the detector of 52 μm *i.e.* 1.9 and 3.8 pixels with the Tektronic and the EEV CCD respectively. The resolution, as measured on the night sky lines, was ∼ 3.4 Å FWHM.

The spectra were flux calibrated using the standard stars given in Table 1, taken from Oke (1974), Stone (1977), Oke & Gunn (1983) and Massey et al. (1988).

The spectra were analysed as described in Véron et al. (1980; 1981a, b) and Gonçalves et al. (1999a). Briefly, the three emission lines, Hα and [N II]$\lambda\lambda$6548,6583 (or Hβ and [O III]$\lambda\lambda$4959, 5007) were fitted by one or several sets of three Gaussian components; the width and redshift of each component in a set were forced to be the same and the intensity ratios of the [N II] and [O III] lines were taken to be equal to their theoretical values. The broad Balmer components were fitted by one or several Gaussian or Lorentzian profiles.

Nineteen galaxies turned out to have been misidentified as NLS1s; their spectra will be published in Véron-Cetty et al. (2001). The 64 others are listed in Table 2.

Before analysing our blue spectra, the Fe II multiplets were removed following the method described in Boroson & Green (1992). This consists of subtracting a suitable fraction of a Fe II template from the NLS1 spectrum so that the flux and width of the Hβ and [O III] lines are no longer affected by the underlying multiplet emission. Such a template is usually obtained by taking a high signal-to-noise spectrum of I Zw 1, an NLS1 showing strong narrow Fe II emission, from which the Hβ and [O III] lines are carefully removed. We have observed I Zw 1 with the same instrumental setting as the rest of the galaxies in our sample and used it to build an Fe II template, following this method.

Our spectra are shown in Figs. 1 to 5.

The Fe II strength is usually quantified by R_{4570} = Fe II λ4570/Hβ, *i.e.* the ratio of the fluxes of the λ4570 Å blend measured between λ4434 and λ4684 and of Hβ, including the narrow component (Boroson & Green 1992).

We have measured the Hβ equivalent width (EW) and the ratio R_{4570} for all objects in our sample. Figure 6 shows plots of our measurements *vs* published ones for the Hβ EW (a) and R_{4570} (b). Our values of the Hβ EW are in good agreement with those of Boroson & Green (1992); the ratios for the 13 objects in common have a mean value of 1.0 with a dispersion of 12%. Our values are also in good agreement with those of Goodrich (1989) with however a larger dispersion (40%); this could be due partly to variability. Our measurements of R_{4570} are 25% lower than the values published by Boroson & Green (1992) (13 objects in common) and 30% lower than those of Goodrich (1989) (10 objects); in both cases the dispersion is ∼25%. A significant difference exists for NGC 4051.

3. Results and discussion

3.1. The broad line region

3.1.1. High- and low-ionization lines

In Seyfert 1s, the broad emission lines can be separated into two distinct systems: the "high-ionization lines" (HILs): C IV λ1550, He II λ4686, He II λ1640, etc, and the "low-ionization lines" (LILs): Fe II, Mg II λ2800, etc. (Collin-Souffrin & Lasota 1988; Gaskell 2000).

The HILs and LILs show strong kinematic differences (Sulentic et al. 1995). C IV is systematically broader

Table 2. List of NLS1s with z<0.100, B<17.0 and $\delta > -25^{o}$. Col. 1: name, col. 2: short position, col. 3: the Galactic hydrogen column density in units of 10^{20} cm^{-2} col. 4: redshift, col. 5: B magnitude, cols. 6 and 7: FWHM (in km s^{-1}) of the broad component of the Balmer lines, and reference, cols. 8 and 9: *ROSAT* (0.1–2.4 keV) photon index Γ resulting from a power-law fit with Galactic absorption, and reference, col. 10: *ROSAT* X-ray flux in cts s^{-1} in the energy band 0.1–2.4 keV either from the RASS catalogue or from the 1WGA catalogue (*), col. 11: "A" if we have obtained a red spectrum, "B" for a blue spectrum. References: (1) Appenzeller & Wagner 1991; (2) Bade et al. 1995; (3) Bassani et al. 1989; (4) Boller et al. 1992; (5) Boller et al. 1996; (6) Boroson & Green 1992; (7) Boroson & Meyers 1992; (8) Brandt et al. 1995; (9) Ciliegi & Maccacaro 1996; (10) Goodrich 1989; (11) Green et al. 1989; (12) Grupe et al. 1998; (13) Grupe et al. 1999; (14) Leighly 1999b; (15) Maza & Ruiz 1989; (16) Moran et al. 1996; (17) Netzer et al. 1987; (18) Osterbrock 1977a; (19) Osterbrock & de Robertis 1985; (20) Osterbrock & Pogge 1985; (21) Osterbrock & Pogge 1987; (22) Osterbrock & Shuder 1982; (23) Puchnarewicz et al. 1994; (24) Puchnarewicz et al. 1995; (25) Rush et al. 1996; (26) Stephens 1989; (27) Stirpe 1990; (28) Walter & Fink 1993; (29) Wang et al. 1996; (30) Winkler 1992; (31) Yuan et al. 1998; (32) Zamorano et al. 1992; (33) Pfefferkorn et al. 2001.

Name	Position	N_H	z	B	FW		Γ		X	
Mark 335	0003+19	3.8	0.025	13.7	1640	(6)	3.10 ±0.05	(14)	2.48	AB
I Zw 1	0050+12	5.1	0.061	14.0	1240	(6)	3.09 ±0.16	(14)	0.82	AB
Ton S180	0054−22	1.5	0.062	14.4	1000	(30)	3.04 ±0.01	(14)	2.53	AB
Mark 359	0124+18	4.8	0.017	14.2	480	(22)	2.4 ±0.1	(5)	0.61	AB
MS 01442−0055	0144−00	2.8	0.080	15.6	1940	(26)	2.7 ±0.2	(5)	0.14	AB
Mark 1044	0227−09	3.0	0.016	14.3	1280	(10)	3.08 ±0.09	(33)	2.14	AB
HS 0328+0528	0328+05	8.9	0.046	16.7					0.22	AB
IRAS 03450+0055	0345+00	11.1	0.031	16.0	1310	(7)			*0.06	–
IRAS 04312+4008	0431+40	34.5	0.020	15.2	690	(16)	2.8 ±0.6	(4)	0.16	AB
Mark 618	0434−10	5.4	0.036	14.5	2300	(7)	2.72 ±0.15	(25)	0.58	–
IRAS 04416+1215	0441+12	14.1	0.089	16.1	1670	(16)	2.96 ±0.50	(4)	0.16	AB
IRAS 04576+0912	0457+09	13.5	0.037	16.6	1220	(16)		(4)		AB
IRAS 04596−2257	0459−22	3.1	0.041	15.6	1500	(11)			*0.51	–
IRAS 05262+4432	0526+44	38.3	0.032	13.6	700	(16)			0.06	AB
RX J07527+2617	0749+26	5.1	0.082	17.0	1000	(2)	3.00 ±0.26	(2)	0.16	AB
Mark 382	0752+39	5.8	0.034	15.5	1500	(18)	3.09 ±0.23	(33)	0.45	AB
Mark 110	0921+52	1.6	0.036	15.4	2120	(6)	2.35 ±0.05	(29)	1.69	–
Mark 705	0923+12	4.0	0.028	14.9	1990	(6)	2.33 ±0.09	(33)	1.25	AB
Mark 707	0934+01	4.7	0.051	16.3	1320	(6)	2.40	(29)	0.46	AB
Mark 124	0945+50	1.3	0.056	15.3	1400	(18)				AB
Mark 1239	0949−01	4.1	0.019	14.4	910	(20)	2.94 ±0.14	(25)	0.05	AB
IRAS 09571+8435	0957+84	3.9	0.092	17.0	1120	(16)	1.39 ±0.40	(4)	0.07	AB
PG 1011−040	1011−04	4.5	0.058	15.5	1440	(6)				AB
PG 1016+336	1016+33	1.6	0.024	15.9	1600	(21)				AB
Mark 142	1022+51	1.2	0.045	15.8	1620	(6)	3.15 ±0.11	(14)	1.75	AB
KUG 1031+398	1031+39	1.4	0.042	15.6	1500	(24)	4.15 ±0.10	(14)	2.66	AB
RX J10407+3300	1037+33	2.2	0.081	16.5	1700	(2)	2.13 ±0.15	(2)	0.25	AB
Mark 734	1119+12	2.7	0.049	14.6	1820	(6)	3.63 ±0.19	(33)	0.42	AB
Mark 739E	1133+21	2.2	0.030	14.1	900	(17)	2.43 ±0.14	(33)	0.49	AB
MCG 06.26.012	1136+34	1.9	0.032	15.4	1685	(13)	2.77 ±0.08	(9)	0.86	AB
Mark 42	1151+46	1.9	0.024	15.4	670	(20)	2.76 ±0.23	(33)	0.19	AB
NGC 4051	1200+44	1.3	0.002	12.9	990	(22)	2.84 ±0.04	(14)	3.92	AB
PG 1211+143	1211+14	2.8	0.085	14.6	1860	(6)	3.03 ±0.15	(14)	1.56	AB
Mark 766	1215+30	1.8	0.012	13.6	2400	(20)	2.79 ±0.11	(14)	4.71	AB
MS 12170+0700	1216+07	2.2	0.080	16.3						AB
MS 12235+2522	1223+25	1.8	0.067	16.3	1730	(26)	3.9 ±0.3	(5)	*0.52	AB
IC 3599	1235+26	1.4	0.021	15.6	1200	(8)	4.2 ±0.1	(12)	5.10	AB
PG 1244+026	1244+02	1.9	0.048	16.1	830	(6)	3.26 ±0.13	(14)	1.30	AB
NGC 4748	1249−13	3.6	0.014	14.0	1100	(19)	2.46 ±0.15	(26)	0.97	AB
Mark 783	1300+16	2.0	0.067	15.6	1900	(20)			0.29	AB
R 14.01	1338−14	7.6	0.042	14.6	1790	(15)			0.31	AB
Mark 69	1343+29	1.1	0.076	15.9	1500	(18)			0.26	AB
2E 1346+2646	1346+26	1.1	0.059	16.5			2.68 ±0.2	(23)	*0.16	AB
PG 1404+226	1404+22	2.0	0.098	15.8	880	(6)	4.04 ±0.20	(29)	0.45	AB
Mark 684	1428+28	1.5	0.046	14.7	1400	(21)	2.4 ±0.2	(12)	0.58	AB
Mark 478	1440+35	1.0	0.077	14.6	1450	(6)	3.06 ±0.03	(14)	5.78	AB
PG 1448+273	1448+27	2.7	0.065	15.0	910	(6)	3.17 ±0.32	(28)	0.78	AB

Table 2. (end)

Name	Position	N_H	z	B	FW		Γ		X	
IRAS 15091−2107	1509−21	8.8	0.044	14.8	1480	(10)			0.36	–
MS 15198−0633	1519−06	12.4	0.084	14.9	1304	(1)	3.39 ±0.26	(31)	0.15	A
Mark 486	1535+54	1.8	0.038	14.8	1480	(6)			*0.05	AB
IRAS 15462−0450	1546−04	12.5	0.100	16.4						AB
Mark 493	1557+35	2.0	0.031	15.1	410	(20)	2.84 ±0.14	(33)	0.52	AB
EXO 16524+3930	1652+39	1.7	0.069	16.7	1000	(3)	2.7 ±0.2	(5)	0.10	AB
B3 1702+457	1702+45	2.2	0.060	15.1	490	(16)	2.37 ±0.18	(14)	0.91	AB
RX J17450+4802	1743+48	3.1	0.054	15.9	1600	(2)	2.64 ±0.13	(2)	0.27	B
Kaz 163	1747+68	4.4	0.063	15.0	1260	(10)	2.76 ±0.03	(14)	0.21	AB
Mark 507	1748+68	4.3	0.053	15.4	965	(10)	1.68 ±0.16	(14)	*0.03	AB
HS 1817+5342	1817+53	4.9	0.080	15.2					0.48	AB
HS 1831+5338	1831+53	4.9	0.039	15.9					0.06	AB
Mark 896	2043−02	4.0	0.027	14.6	1330	(27)	3.38 ±0.05	(33)	0.44	AB
MS 22102+1827	2210+18	6.2	0.079	16.7					0.13	AB
Akn 564	2240+29	6.4	0.025	14.2	750	(27)	3.47 ±0.07	(14)	3.84	AB
HS 2247+1044	2247+10	6.2	0.083	15.8					0.18	AB
Kaz 320	2257+24	4.9	0.034	16.8	1800	(32)			0.53	AB

than Mg II (Mathews & Wampler 1985) or Hβ (Wang et al. 1998) and shows a strongly blueshifted and blue asymmetric profile (Marziani et al. 1996), and He II λ4686 systematically broader than Hβ (Boroson & Green 1992; Peterson et al. 2000). The widths of Hβ and Fe II (Boroson & Green 1992) and of Hβ and C III]λ1909 (Wills et al. 2000) are strongly correlated ; in two NLS1s, Leighly (2001) found that Si III] and C III] have the same width as the LILs; but, if Puchnarewicz et al. (1997) found that the FWHM of Hβ and Mg II are also correlated, they also found that that of C III] and Mg II are not. These observations support the idea of separate HIL and LIL emitting regions although it is not quite clear if C III] belongs to the HIL or to the LIL region.

The Fe II emission in most AGNs is too strong to be explained by photoionization (Phillips 1978b; Kwan et al. 1995); Fe II lines, and the other LILs as well, are more likely to be explained in the framework of collisional models where both the excitation of the lines and the ionization of the elements are due to collisions in a high density optically-thick medium illuminated mainly by hard X-rays; the Fe II emission region has a high density ($10^{10} < N_e < 10^{11}$ or 10^{12} cm^{-3}), a high column density ($N_H > 10^{24}$ cm^{-2}) and a low temperature (7 500 < T < 10 000 K) (Collin-Souffrin et al. 1980; 1988b; Joly 1981; Clavel et al. 1983; Collin-Souffrin & Lasota 1988; Kwan et al. 1995). There is a significant correlation between Si III]λ1892/C III]λ1909 and R_{4570}; Si III and C III have similar ionization potentials, but Si III] has a critical density more than one order of magnitude larger than C III] (1.1×10^{11} and 5×10^{9} cm^{-3} respectively); Si III]/C III] is thus a density indicator and becomes larger when density is higher; Si III]/C III] increases with increasing N_e up to N_e=10^{11} cm^{-3} (Aoki & Yoshida 1999; Wills et al. 1999; Kuraszkiewicz et al. 2000). It seems therefore likely that the C III] line comes from the same high density region as Hβ and Fe II where it is at least partially suppressed by collisions.

HILs are emitted by low-pressure optically thin clouds (density of at most a few 10^9 cm^{-3}) illuminated by a rather soft continuum radiation (UV and soft X-rays) (Collin-Souffrin & Lasota 1988). Collin-Souffrin et al. (1988a) suggested that these lines are produced in clouds undergoing predominantly outward motions along the system axis, the clouds receding from us being hidden by an opaque structure such as the accretion disk. The bipolar outflow could be a hydromagnetically driven wind accelerated radiatively and centrifugally away from the surface of the accretion disk (Emmering et al. 1992; Königl & Kartje 1994; Bottorf et al. 1997; Murray & Chiang 1998).

The broad Balmer lines exhibit a wide variety of profile shapes and a large range in width (Osterbrock & Shuder 1982; de Robertis 1985; Crenshaw 1986; Stirpe 1991; Miller et al. 1992); they are often strongly asymmetric (Corbin 1995). The BLR consists of two components: one Intermediate Line Region (ILR) with line width ∼2 000 km s^{-1} FWHM, with the peak within a few hundred kilometers per second of the systemic redshift, and a Very Broad Line Region (VBLR) with lines of width > 7 000 km s^{-1} and blueshifted by more than 1 000 km s^{-1}; differences in the relative strengths of these components account for much of the diversity of broad line profiles (Wills et al. 1993; Brotherton et al. 1994; Corbin 1995; 1997; Francis et al. 1992). The spectra of the VBLR and ILR are very different (Brotherton et al. 1994); the VBLR and the ILR can probably be identified with the HIL and LIL regions respectively (Puchnarewicz et al. 1997). This is confirmed by variability studies: the profile of the broad emission lines are variable; many of them can be described by two Gaussian components that are nearly stationary in wavelength, and which vary

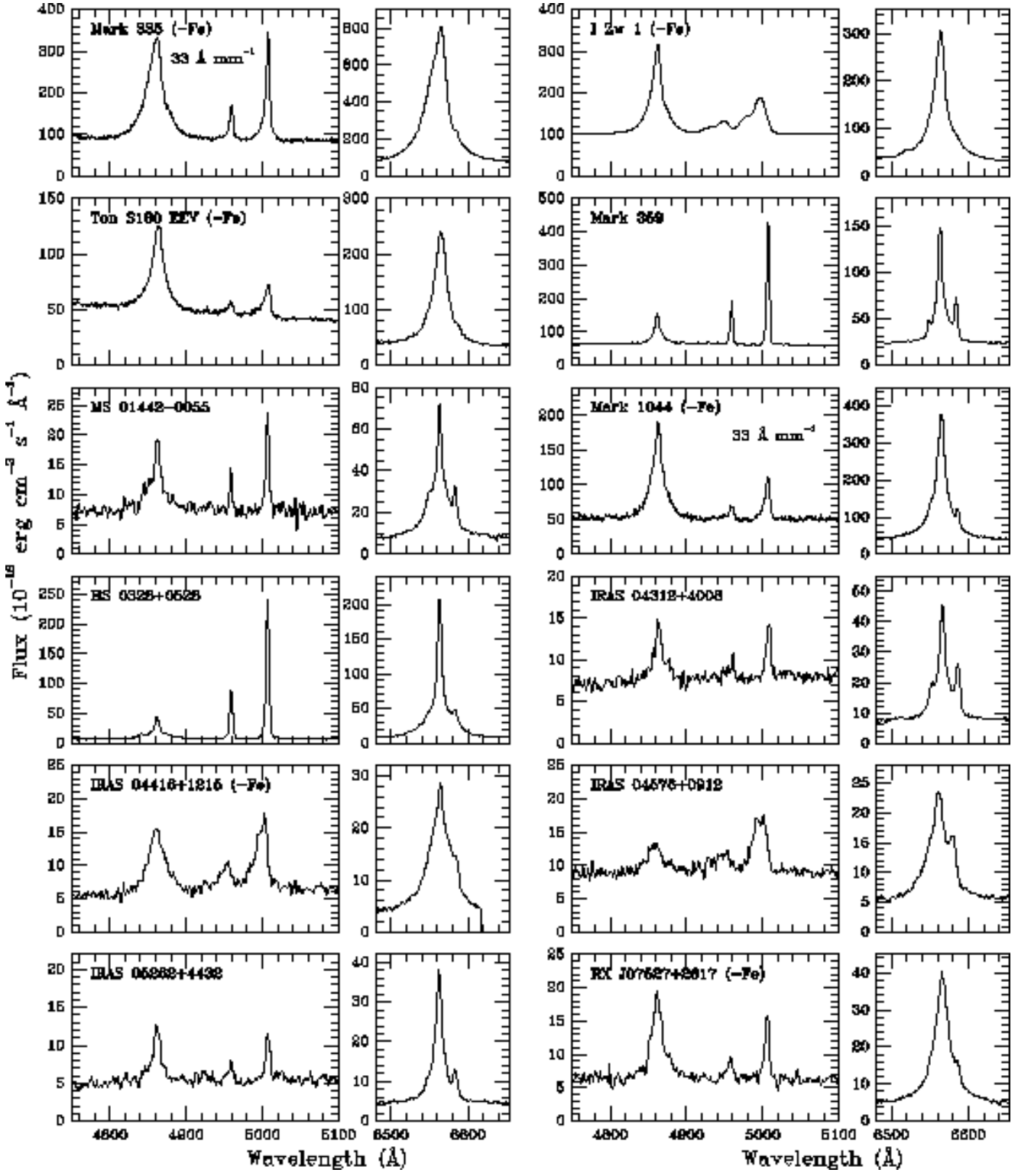

Fig. 1. Deredshifted blue and red spectra of the observed NLS1s.

independently of one another in relative flux (Peterson et al. 1999). This is the case for NGC 5548 (Dumont et al. 1998) and NGC 3516 (Goad et al. 1999) in which the emission lines are best explained by the superposition of an emission line cloud with variable lines and another which shows no variability; the emission spectrum of the non variable cloud is dominated by Balmer lines and Fe II emission. In the case of PG 1416−129, the broad Hβ component (4 000 km s^{-1} FWHM) is strongly variable while the very broad component (13 000 km s^{-1} FWHM) has a much smaller amplitude (Sulentic et al. 2000b).

LILs could be produced in the outer part of the disk itself as a result of energy reflected from the flow above the

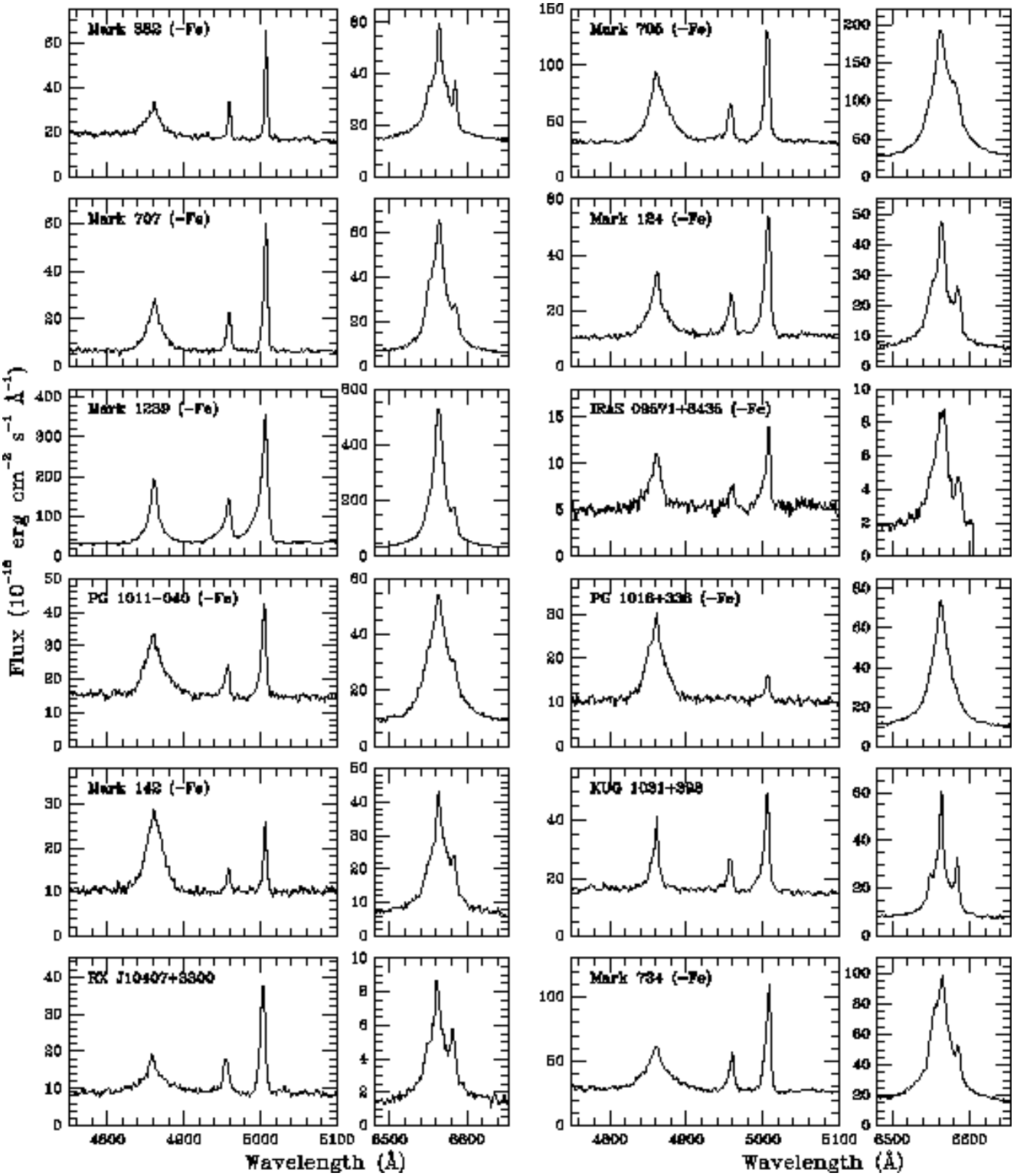

Fig. 2. Deredshifted blue and red spectra of the observed NLS1s (continued).

disk (Collin-Souffrin et al. 1988a). The profile of the lines produced in a disk are generally not double peaked, except if the radius of the disk is small ($\sim 10^3$ R_G where R_G is the gravitational radius of the central BH), in which case the line intensities are small, the line profiles are U-shaped and very broad; if the disk radius is large ($>10^4$ R_G), the line intensities are large and their profile generally single peaked; the spectrum consists mainly of LILs and can be a major part of the broad line emission (Dumont & Collin-Souffrin 1990); these lines are, under certain conditions, more similar to a Lorentzian than to a Gaussian (see their Fig. 4b).

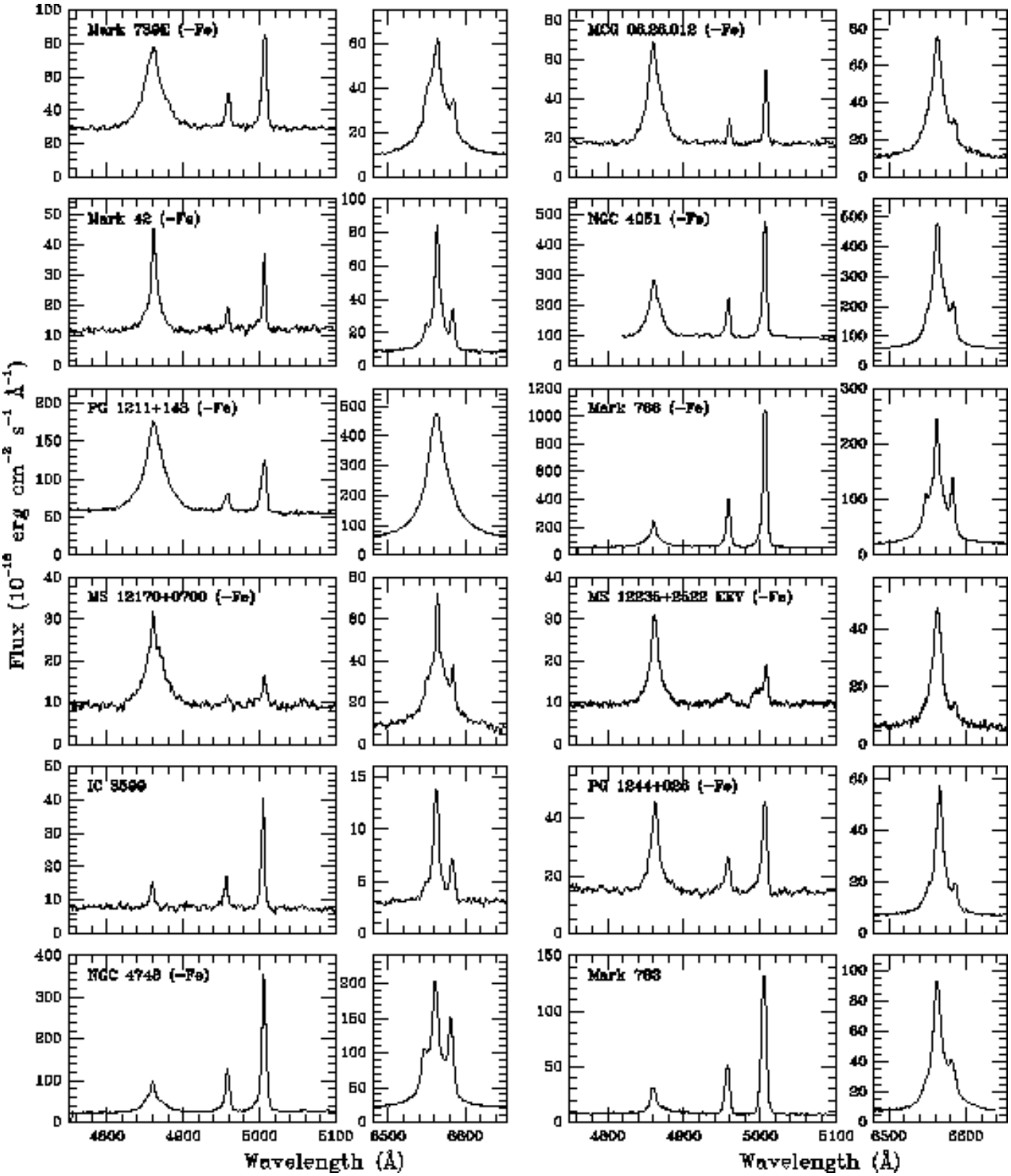

Fig. 3. Deredshifted blue and red spectra of the observed NLS1s (continued).

3.1.2. On the profile of the NLS1 broad lines

According to Moran et al. (1996) and Leighly (1999b), many NLS1s have symmetric emission lines with more nearly Lorentzian than Gaussian profiles. However Rodríguez-Ardila et al. (2000b) claimed that Lorentzian profiles are not suited to represent the NLS1 broad emission-lines; this conclusion is based on the fact that these authors were unable to get a good fit when using a single Lorentzian for each of the emission lines; however, there is a major inconsistency in their procedure: they assumed that the Balmer lines (either Hα or Hβ) had a pure Lorentzian profile, not allowing for the presence of a nar-

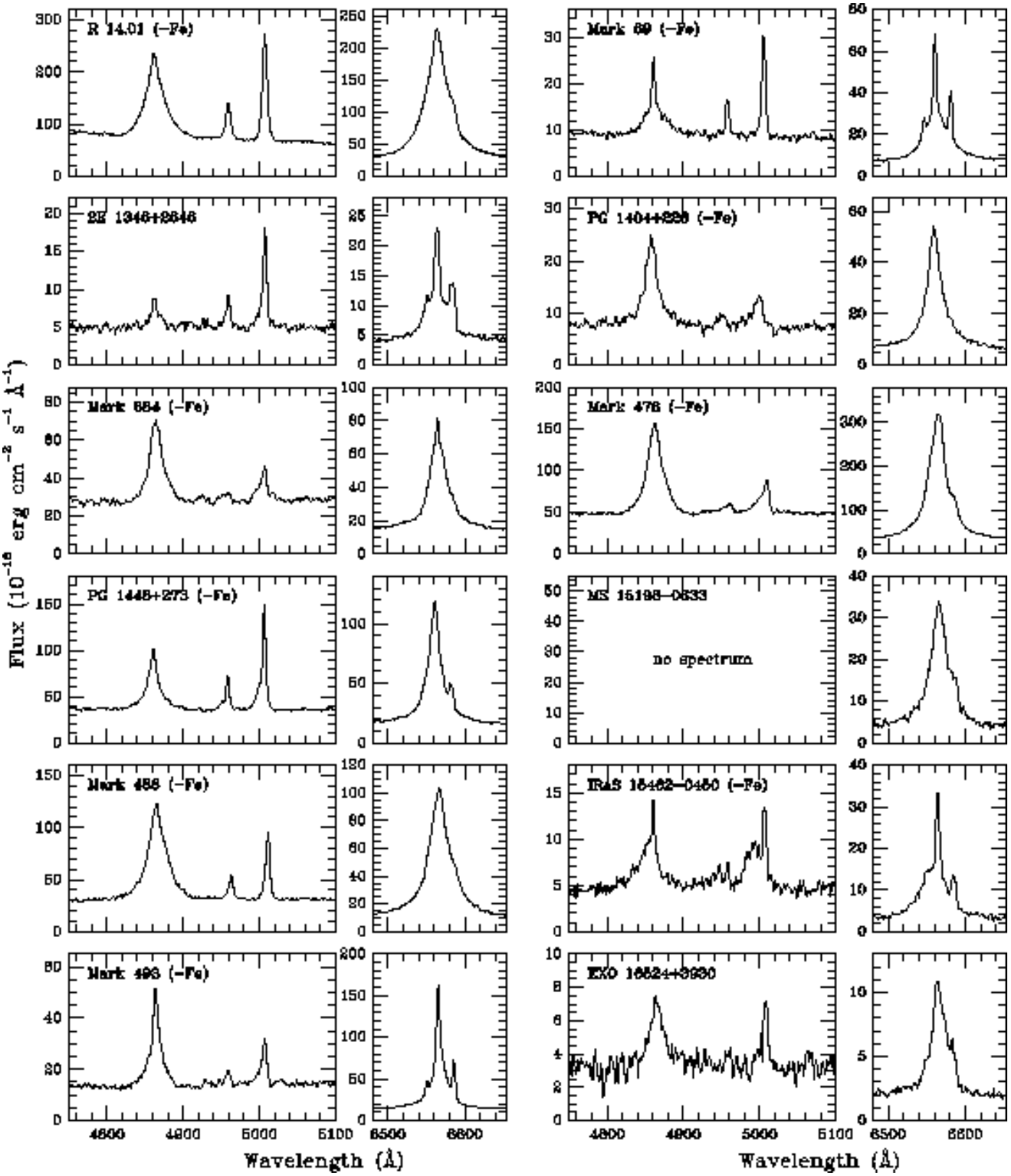

Fig. 4. Deredshifted blue and red spectra of the observed NLS1s (continued).

row component. It so happens that one of the objects they present as an example of the poor results obtained when fitting the emission lines with Lorentzians (Mark 1239) is one of those for which we obtain a very good fit using a Lorentzian profile for the broad Balmer line components in addition to a narrow component having the same Gaussian profile as the forbidden lines.

Although not all broad Balmer components in our sample are well fitted by a single Lorentzian, this is true in most cases (Table 3 lists, for all observed objects, the FWHM of the Hα and Hβ broad components obtained

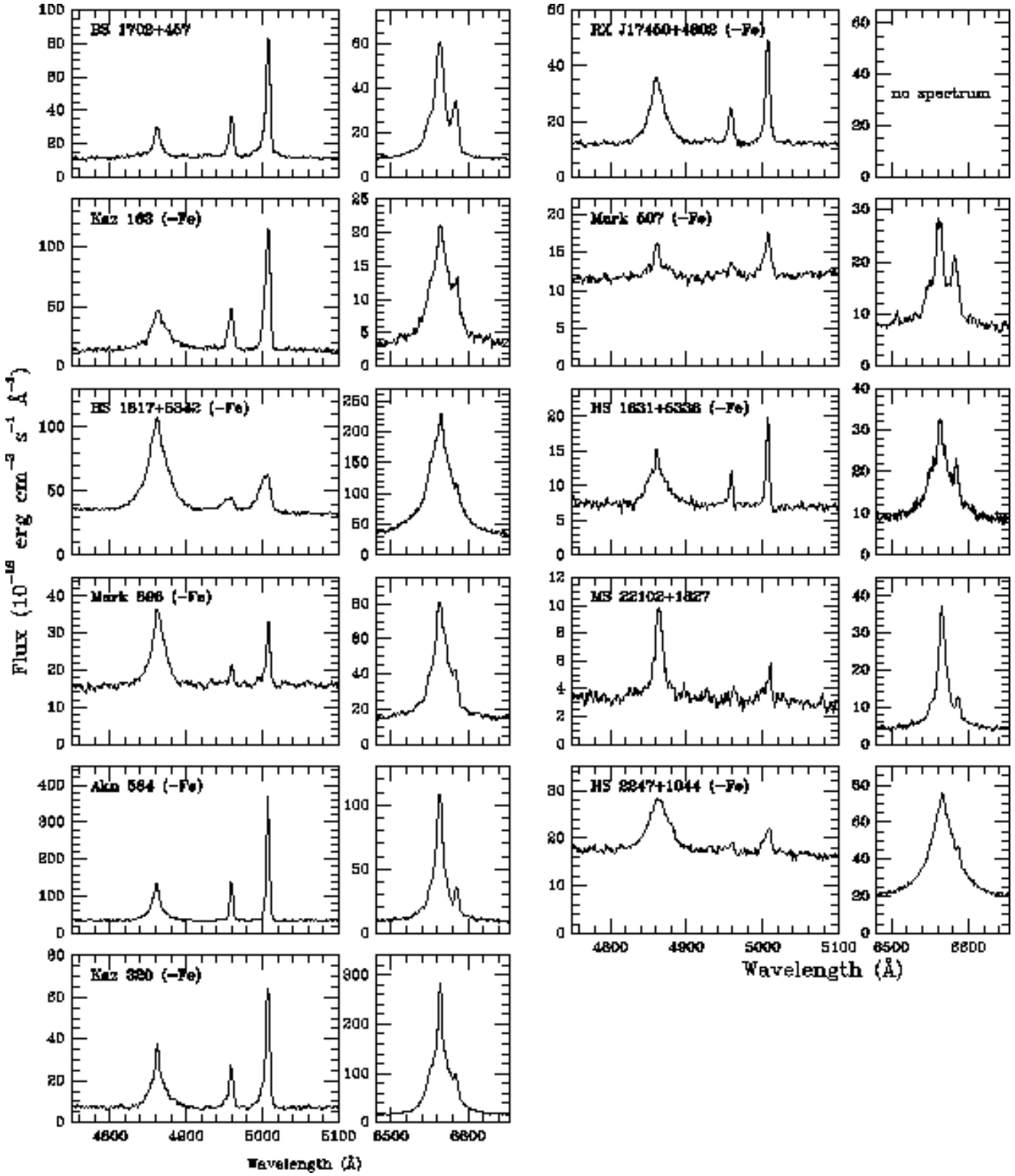

Fig. 5. Deredshifted blue and red spectra of the observed NLS1s (end).

by using a single Lorentzian). As an illustration, we show in Fig. 7 the blue and red spectra of four objects fitted by a single broad Gaussian and by a single broad Lorentzian; the narrow lines have been fitted either by a single Gaussian or by two Gaussians. In three cases, the fit of the red spectra is significantly better with a Lorentzian than with a Gaussian, as judged from the residuals. The improvement of the fit of the blue spectra with a Lorentzian is significant only for PG 1244+026. But, in all cases, the Lorentzian fit leads to λ6583/Hα and λ5007/Hβ ratios which are more similar to the values expected for Seyfert 2 nebulosities (see below).

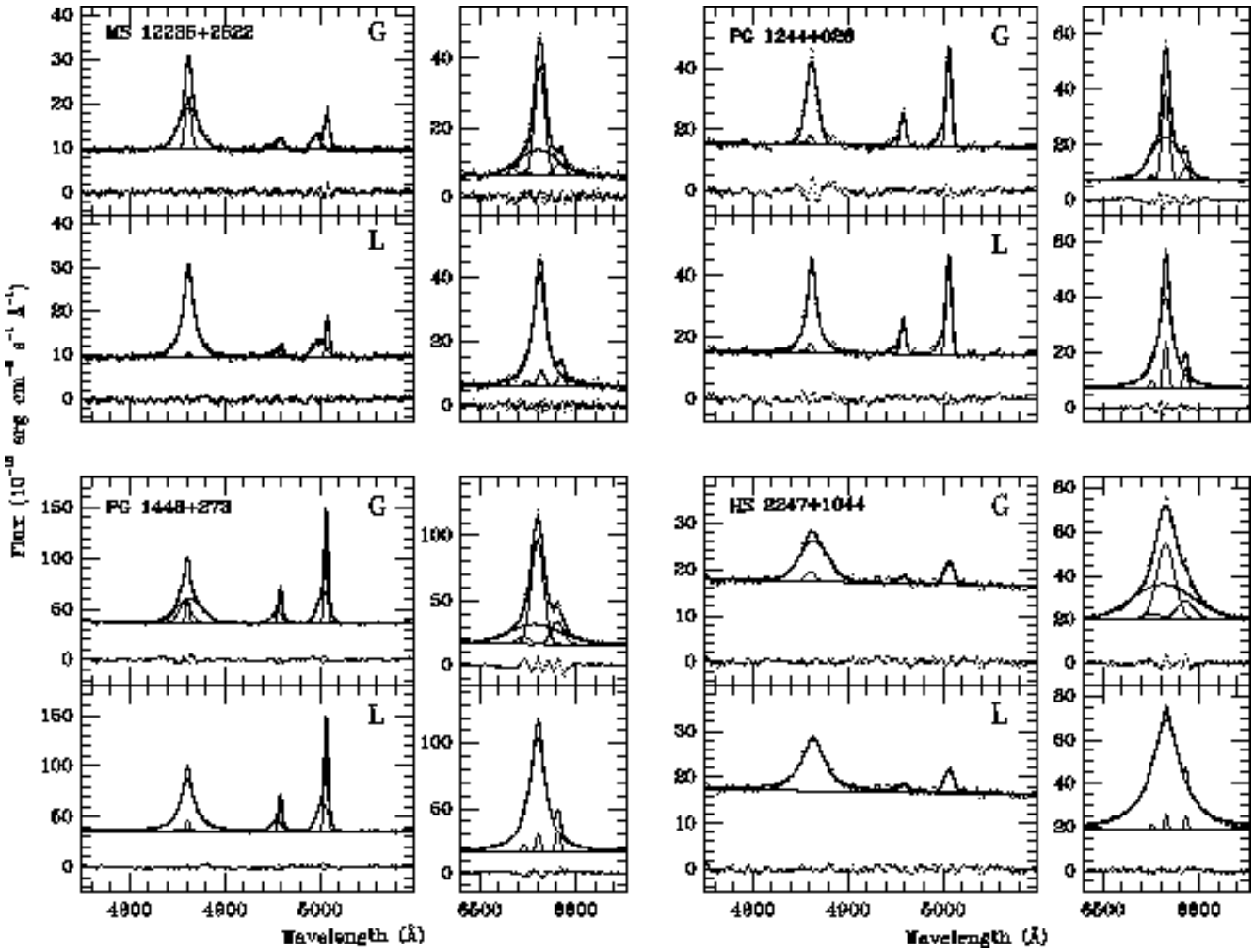

Fig. 7. Deredshifted blue and red spectra of four NLS1 galaxies in our sample. The data points were fitted by a set of narrow Gaussian profiles, reproducing the narrow emission lines, plus a Gaussian (G) or Lorentzian (L) profile, to fit the broad Balmer component. The individual profiles are represented by a thin solid line, the total fit by a thick solid line and the differences between the data and the fit (the residuals) by the lower dotted line.

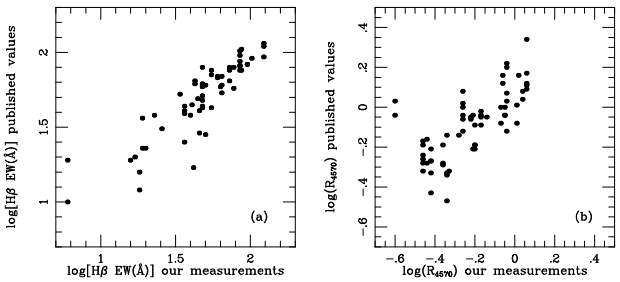

Fig. 6. (a) Comparison between our measurements of the Hβ EW and the published ones. (b) Comparison between our measurements of R_{4570} and the published ones.

The use of a Lorentzian rather than a Gaussian leads, for the NLR of most NLS1s, to line ratios typical of classical Seyfert 2s which strongly confirms that these broad Balmer components have a profile which is genuinely more similar to a Lorentzian. We give in Table 4 the FWHM of the broad Gaussian and Lorentzian profiles for these four objects; we first note that the FWHM of the Hα and Hβ Lorentzians are equal within ∼10%, while the Hα FWHM of the Gaussians are on average 50% larger than the Hβ FWHM; this probably reflects the better quality of the fits obtained with Lorentzians. The FWHM of the Gaussians are systematically larger than the FWHM of the Lorentzians; in particular, HS 2247+1044 would not be classified as an NLS1 from a Gaussian fit.

The fact that the broad Balmer lines in NLS1s have a nearly Lorentzian profile seems to suggest that they are produced in a large disk without the contribution from an outflowing component. However, the high ionization UV emission lines in the spectrum of NLS1s appear to be significantly broader than Hβ (Rodríguez-Pascual et al. 1997; Kuraszkiewicz et al. 2000; Wills et al. 2000). In addition, Leighly (2001) showed that the high-ionization UV emission lines in two NLS1s (IRAS 13224−3809 and 1H 0707−495) are much broader and strongly blueshifted than the low-ionization lines. These observations suggest

Table 4. FWHM of the broad component of the Hα and Hβ lines when fitted either by a Gaussian or a Lorentzian profile. Col. 1: name, cols. 2 and 3: FWHM (km s^{-1}) of the broad Hα and Hβ lines fitted with a Gaussian, col. 5: ratio (R) of the FWHM of Hα to Hβ, cols. 6 and 7: FWHM (km s^{-1}) of the broad Hα and Hβ lines fitted with a Lorentzian, col. 8: ratio of the FWHM of Hα to Hβ.

Name	Gaussian fit			Lorentzian fit		
	Hα	Hβ	R	Hα	Hβ	R
	FWHM			FWHM		
MS 12235+2522	2100	1585	1.32	705	800	0.88
PG 1244+026	1625	945	1.72	820	740	1.11
PG 1448+273	3000	1890	1.59	915	1050	0.87
HS 2247+1044	3410	2280	1.50	1625	1790	0.91

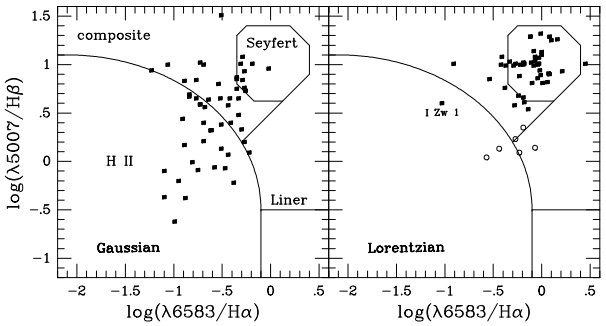

Fig. 8. Diagnostic diagrams for the narrow line region of the objects in our sample. In the left panel, the line ratios have been derived by fitting the broad Balmer components with a single Gaussian, while in the right panel we have used a single Lorentzian. In the right panel, Seyfert 2s are shown by black squares and H II regions by open circles.

that, in NLS1s, the outflowing component exists but is relatively weak, its contribution being negligible in the optical range.

3.2. The narrow line region

3.2.1. The line ratios of the narrow line region

As we have seen above, for all objects for which a single Lorentzian gave a good fit to the broad Balmer component, we also made a fit with a single Gaussian. In this way, we obtained two sets of line ratios (λ5007/Hβ and λ6583/Hα) which are plotted in Fig. 8 (when the signal to noise ratio is low, the fit with a single broad Hβ Lorentzian sometimes gives a low value for the λ5007/Hβ ratio; in these cases, when forcing this ratio to be equal to 10, the fit is not worse as illustrated for IRAS 05262+4432 in Fig. 9). The left panel shows the ratios obtained by fitting the broad Balmer component with a Gaussian; the right panel, the ratios obtained with a Lorentzian. While, in the left panel, many points are located in the H II region or composite domain (Gonçalves et al. 1999a), in the right panel, most of the points are in the Seyfert 2 region; one object (HS 0328+0528) belongs to the rare class of weak-[N II] Seyfert galaxies (Gonçalves et al. 1999a) while six (Mark 42, MS 12170+0700, Mark 69, Mark 684, IRAS 15462−0450 and Mark 507) have an emission line component which falls in or near the H II region domain and is a genuine H II region; they are shown as open circles; these objects are most probably composite type objects similar to those described by Véron et al. (1981b) and Gonçalves et al. (1999a). The fit of the broad component of I Zw 1 with a single component is clearly unsatisfactory; we got a better fit with two Lorentzians which puts the representative point of the narrow line region in the Seyfert 2 area.

In contrast, Rodríguez-Ardila et al. (2000b) found that the λ5007/H$\beta_{\rm n}$ ratio emitted in the NLR of NLS1s varies from 1 to 5, instead of ∼10 for BLS1s. This is most probably due to the fact that they modelled the broad Balmer component with a Gaussian rather than a Lorentzian. On the other hand, Nagao et al. (2001) showed that the line ratios [O I]λ6300/[O III]λ5007 and [O III]λ4363/[O III]λ5007 are statistically indistinguishable in NLS1s and BLS1s.

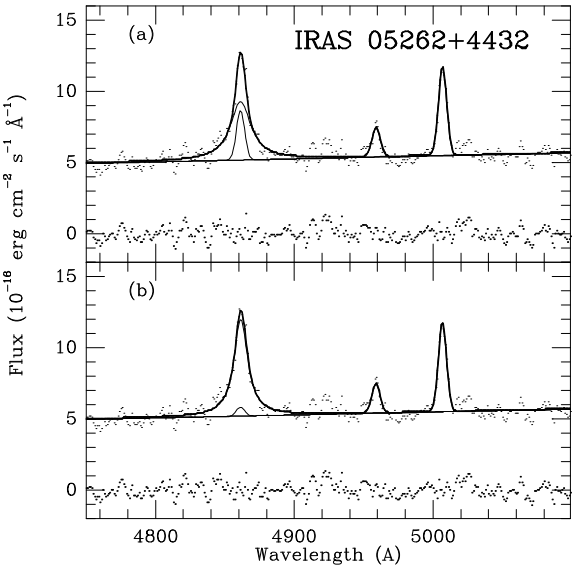

Fig. 9. In (a), we have fitted the blue spectrum of IRAS 05262+4432 with a set of Gaussian profiles for the narrow lines plus a single Lorentzian profile for the broad component of Hβ; in (b), we forced the λ5007/Hβ ratio to be equal to 10. Examination of the residuals shows that the two solutions have equal merits.

3.2.2. The kinematics of the narrow line region

The majority of the profiles of the [O III] lines in Seyfert 1s are markedly asymmetric, exhibiting a sharper falloff to the red than to the blue (Heckman et al. 1981; Vrtilek &

Table 3. Line properties of the 59 observed NLS1s (H II components have been systematically removed). Col. 1: name, col. 2: R_{4570}, ratio of the Fe II to the total Hβ fluxes, cols. 3 and 4: FWHM (in km s^{-1}) of the broad Hα and Hβ lines fitted with a Lorentzian profile, col. 5: EW (Å) of the broad Hβ component, col. 6: R_{5007}, ratio of the λ5007 to the total Hβ fluxes, col 7: FWHM (corrected for instrumental broadening) of the [O III] line, cols. 8 and 9: FWHM of the individual components (F1 and F2) of the [O III] lines, col. 10: velocity difference between the two [O III] components (broad–narrow), col. 11: intensity ratio of the two [O III] components (broad/narrow). a: a good fit can only be obtained with two broad components, a Lorentzian and a Gaussian or two Lorentzians. b: the broad Hβ component is weak.

Name	R_{4570}	FWHM (L)		EW	R_{5007}	FWHM	FW1	FW2	ΔV	F2/F1
		Hα	Hβ	Hβ_{br}		λ5007				
Mark 335	0.38	a	a	86	0.25	280	245	910	−190	1.23
I Zw 1	1.14	a	a	48	0.44	1660	1040	1070	−1180	0.43
Ton S180	1.03	1250	1085	46	0.18	675	435	1060	−465	1.00
Mark 359	<0.5	830	900	18	1.32	180				
MS 01442−0055	<0.6	1260	1100	35	0.35	240				
Mark 1044	0.61	905	1010	63	0.15	420	335	720	−340	0.69
HS 0328+0528	<0.6	1455	1590	79	1.67	220				
IRAS 04312+4008	<1.4	1060	860	16	0.35	380				
IRAS 04416+1215	1.14	1500	1470	55	0.67	1320	650	1790	−480	1.95
IRAS 04576+0912	<1.0	1100	1210	13	1.40	1290	380	1260	−500	6.40
IRAS 05262+4432	1.09	695	740	23	0.35	365				
RX J07527+2617	0.71	1080	1185	50	0.21	400				
Mark 382	<0.8	1270	1280	20	0.56	155				
Mark 705	0.36	1745	1790	85	0.41	365	365	1630	−290	0.62
Mark 707	0.47	1180	1295	102	0.53	315				
Mark 124	0.60	1645	1840	43	0.72	540	380	935	−335	0.75
Mark 1239	0.63	905	1075	78	1.29	630	400	1395	−475	1.16
IRAS 09571+8435	1.05	1270	1185	26	0.53	430	240	845	−370	1.07
PG 1011−040	0.46	1370	1455	41	0.33	400				
PG 1016+336	0.60	1205	1590	65	0.06	315				
Mark 142	0.92	1335	1370	60	0.14	260				
KUG 1031+398	<1.5	1225	935	17	0.93	1000	315	1115	−280	1.27
RX J10407+3300	<0.6	1425	1985	32	0.75	460				
Mark 734	0.67	1345	1825	45	0.49	450	180	525	−230	1.41
Mark 739E	0.61	1415	1615	63	0.23	380				
MCG 06.26.012	0.52	1070	1145	83	0.14	220				
Mark 42	0.90	805	865	36		220				
NGC 4051	0.25	970	1120	50	0.55	300	200	665	−175	0.65

Carleton 1985; Whittle 1985a; Veilleux 1991b); these profiles often have a two component structure with a narrow core superposed on a broader, blueshifted base (Heckman et al. 1981; Leighly 1999b); it seems that the velocity of the core is equal to the systemic velocity of the galaxy (Heckman et al. 1981; 1984; Whittle 1985a).

Many Seyferts have an "ionization cone" appearing as either one- or two-sided structures emanating from the active nucleus; when single (one-sided) cones are seen, they generally project against the far side of the galaxy disk, suggesting that the counter cone is present but obscured by dust in the disk (Pogge 1989; Wilson et al. 1993; Wilson 1994). Colbert et al. (1996) suggested that more than 25% of Seyfert galaxies have good evidence (from the kinematics of the Hα and [N II] lines) for minor axis galactic outflows. Crenshaw et al. (1999) showed, from the observation of UV absorption lines (mainly C IV and N V), that large scale outflows with a velocity of a few hundreds km s^{-1} are common in Seyfert galaxies. High spatial resolution spectroscopic observations of the nuclear emission lines of NGC 1068 (Crenshaw & Kraemer 2000) and NGC 4151 (Crenshaw et al. 2000; Kaiser et al. 2000) give strong support for biconical radial outflows in these objects.

Whittle et al. (1988), Storchi-Bergmann et al. (1992), Arribas & Mediavilla (1993) and Kaiser et al. (2000) showed that the AGN NLRs have two line-emitting constituents: the "[O III] components" (the broad blueshifted bases of the [O III] lines; Heckman et al. 1981; Vrtilek 1985; Whittle 1992; Christopoulou et al. 1997), to be identified with the biconical structure and which are outflowing from the nucleus with a speed of a few hundreds km s^{-1}, and the "ambient [O III] emission" which is more widely distributed and shows normal galactic rotation. A detailed kinematic study of the emission line gas in the Seyfert galaxy NGC 2992 shows the presence of both a disk component which is well modeled by pure circular rotation and an outflowing component distributed into two wide cones (Veilleux et al. 2001). Smith (1993) suggested

Table 3. (end)

Name	R_{4570}	FWHM (L)		EW	R_{5007}	FWHM	FW1	FW2	ΔV	F2/F1
		Hα	Hβ	Hβ_{br}		λ5007				
PG 1211+143	0.44	1400	1975	95	0.12	510				
Mark 766	0.35	1150	1630	55	1.83	330	220	710	−90	0.73
MS 12170+0700	0.65	1405	1765	79		365				
MS 12235+2522	0.62	705	800	43	0.24	875	240	905	−570	1.34
IC 3599		500	–	6	3.23	280				
PG 1244+026	1.09	820	740	36	0.47	415	330	740	−390	0.40
NGC 4748	0.55	1400	1565	65	1.34	365	295	1170	−150	0.49
Mark 783	<0.5	1510	1655	42	2.29	430				
R 14.01	0.44	1470	1605	85	0.28	430				
Mark 69	0.59	1445	1925	34		315				
2E 1346+2646		1235	b		2.40	330	180	950	−105	1.07
PG 1404+226	0.85	1015	1120	65	0.19	950				
Mark 684	0.91	a	1150	40	0.14	1290				
Mark 478	0.55	1190	1270	72	0.17	920	365	1230	−475	2.05
PG 1448+273	0.73	915	1050	36	0.61	315	155	890	−215	1.11
MS 15198−0633		1115	–	–						
Mark 486	0.46	1400	1680	123	0.13	400				
IRAS 15462−0450	0.59	1830	1615	41	0.62	1600				
Mark 493	0.87	870	740	46	0.26	450	315	845	−400	0.75
EXO 16524+3930	<0.9	1025	1355	39	0.21	400				
B3 1702+457	<1.2	930	975	19	2.03	365	295	1200	−280	0.56
RX J17450+4802	0.78	–	1355	48	0.45	400				
Kaz 163	0.35	1325	1875	87	0.70	480				
Mark 507	1.94	1205	1565	6	0.50	1025				
HS 1817+5342	0.59	1625	1615	79	0.20	1000	570	1215	−375	2.21
HS 1831+5338	0.74	1470	1555	32	0.30	240				
Mark 896	0.50	1015	1135	32	0.19	315				
MS 22102+1827	<1.2	820	690	42	0.16	890				
Akn 564	0.67	710	865	48	0.92	220				
HS 2247+1044	1.11	1625	1790	30	0.12	710				
Kaz 320	0.49	1160	1470	85	0.70	350	260	830	−275	0.57

that the "[O III] component" could be accelerated outwards by a supersonic wind generated by the active nucleus. The relative intensity of the two components varies widely from object to object.

High-ionization lines ([Fe VII], [Fe X] and [Fe XI]) are often present in emission in NLS1s; these coronal lines tend to be blueshifted relative to, and broader than, the low-ionization lines; the systematic blueshift indicates an outflow of the gas emitting these features (Grandi 1978; Erkens et al. 1997).

There is a strong correlation between the [O III]λ5007 line width and luminosity (Whittle 1985b). The [O III] FWHM is correlated with the absolute magnitude of the galaxy bulge (Véron & Véron-Cetty 1986) and the observed galaxy rotation (Véron 1981; Whittle 1992) showing that gravity plays a dominant role in the NLR of most objects, at least in the "ambient [O III] emission" region which dominates in most AGNs.

For a number of objects in our sample (30), the fit of the [O III] lines with a single Gaussian was poor, either because of the simultaneous presence on the slit of a H II region (6), or because the lines are asymmetrical with a blue wing (24); in these last cases, we fitted them with two Gaussians following the procedure described in section 2; as a result, we found a red component with a FWHM in the range 180–650 km s^{-1} and a blue component with a FWHM in the range 525–1 790 km s^{-1}, blueshifted by 90 to 570 km s^{-1} with respect to the red component (Table 3; in this table, the [O III] FWHM have been corrected for the instrumental profile); there is one exception, I Zw 1, for which the red component is exceptionally broad (1 040 km s^{-1} FWHM) and the blue component is blueshifted by 1 180 km s^{-1}. This is in agreement with previous findings.

For the objects requiring an additional [O III] component, the associated Hβ line was often very weak; as a result, the fitting routine sometimes gave a negative flux; in such cases, we set the ratio λ5007/Hβ to 10, the mean value for Seyfert galaxies. This is a common procedure used to prevent the fitting routine to yield non-physical values whenever the line intensities are too small to be disentangled from the noise.

The soft X-ray photon index is available for 41 of the objects for which we have a blue spectrum. Twenty of them have $\Gamma > 2.9$, 21 have a smaller value; among the

20 objects with a steep soft X-ray spectrum, 12 have a blueshifted [O III] component, while only eight of the other set have such a component; moreover, two of the eight steep X-ray spectrum objects without a blueshifted component (PG 1404+226 and RXS J07527+2617) have an optical spectrum with a poor signal to noise ratio and relatively broad [O III] lines (950 and 400 km s^{-1} respectively) so that the presence of a blueshifted component could have been overlooked. So there is a weak, statistically unsignificant, trend for the objects with a soft X-ray excess to have an outflowing [O III] component. It is interesting to remark that Erkens et al. (1997) have found that strong coronal lines occur predominantly in objects with the steepest soft X-ray spectra and that these lines are relatively broad and bluehifted. The FWHM and velocity shifts are comparable for the blueshifted [O III] lines and the coronal lines. Could these lines all come from the same emitting clouds?

3.3. The Fe II emission

3.3.1. Correlation between the strength of the Fe II emission and the width of the broad Hβ component

Typical AGNs have R_{4570} ∼0.4 with ∼90% of objects in the range 0.1 to 1 (Osterbrock 1977a; Bergeron & Kunth 1984). Moderately strong Fe II emission ($R_{4570} > 1$) occurs in perhaps 5% of all objects (Lawrence et al. 1988). A few superstrong Fe II emitters ($R_{4570} > 2$) have been found (Lawrence et al. 1988; Lipari et al. 1993; Lipari 1994; Moran et al. 1996; Xia et al. 1999); they are listed in Table 5. They are roughly an order of magnitude rarer.

Table 5. Known superstrong Fe II emitters ($R_{4570} > 2$)

Name	Position	R_{4570}	H$\beta_{\rm br}$ FWHM km s^{-1}
IRAS 04312+4008	0431+40	2.4	1230
IRAS 07598+6508	0759+65	2.6	3200
IRAS 10026+4347	1002+43	2.0	2500
IRAS 11598−0112	1159−01	3.3	780
Mark 231	1254+57	2.1	3000
IRAS 13224−3809	1322−38	2.4	650
Mark 507	1748+68	2.9	965
IRAS 18508−7815	1850−78	2.4	3100
IRAS 23410+0228	2341+02	4.0	970

Wills (1982) was the first to suggest that R_{4570} is roughly inversely proportional to line width (FWHM of the broad Hβ component). Gaskell (1985) showed that R_{4570} increases dramatically for FWHM < 1 600 km s^{-1}, but is relatively constant for FWHM > 1 600 km s^{-1}. Zheng & Keel (1991) found that for AGNs with FWHM > 6 000 km s^{-1}, the mean value of R_{4570} is 0.21, less than half of that of the other objects, confirming that strong Fe II emission is not found in objects showing very broad emission lines; they showed that this is not an artifact resulting from blending of the Fe II lines when they are broad. Boroson & Green (1992), followed by Wang et al. (1996) and Rodríguez-Ardila et al. (2000a), confirmed the existence of a strong anticorrelation between R_{4570} and Hβ FWHM. This anticorrelation could be due either to the existence of an anticorrelation between Fe II EW and Hβ FWHM (Zheng & O'Brien 1990; Boroson & Green 1992) or of a correlation between Hβ EW and FWHM (Osterbrock 1977a; Gaskell 1985; Goodrich 1989).

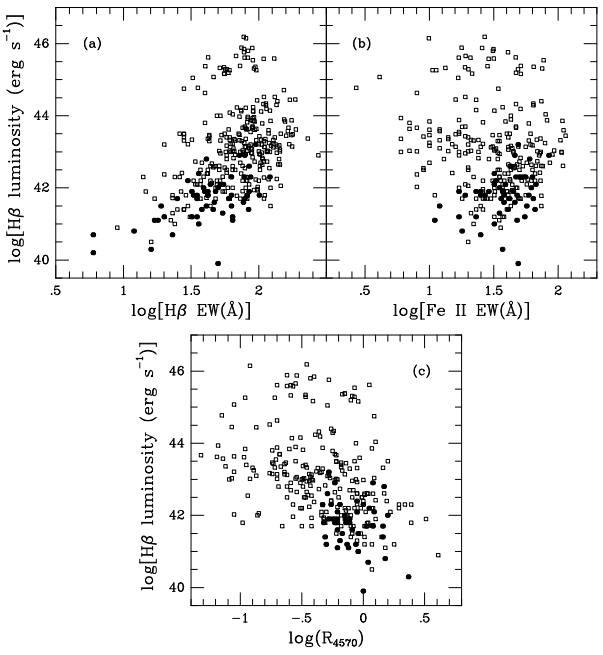

Fig. 10. Plots of the broad Hβ luminosity: in (a) *vs* the EW of the broad Hβ component; the two parameters are highly correlated (r=0.43) for low luminosity objects (L(Hβ) <$10^{42.5}$ erg s^{-1}); but the Hβ EWs saturate at ∼100 Å for larger luminosity objects; in (b), *vs* the Fe II EW; it is a scatter diagram (r=0.20); in (c) *vs* R_{4570}. The anticorrelation observed (r=0.42) is clearly due to the weakness of Hβ in the low luminosity objects rather than to the strength of R_{4570}. Several samples of Seyfert 1s have been used; our own is shown as filled circles; others (see text) are shown as open squares.

We have plotted in Fig. 10 the broad Hβ luminosity *vs* the H$\beta_{\rm br}$ EW, the Fe II EW and R_{4570} for all objects in our sample and in those of Boroson & Green (1992), Brotherton (1996), Moran et al. (1996), Marziani et al. (1996), Corbin & Boroson (1996), Corbin (1997), Grupe et al. (1999) and McIntosh et al. (1999); Grupe et al. reported the EW of the whole Fe II complex from 4250 to 5880 Å; Leighly (1999b) used 30% of this value; we used 20%. This figure clearly shows that the anticorrelation between Hβ luminosity and R_{4570} (r=0.42) is the result of the correlation between Hβ luminosity and EW (r=0.43) as there is no correlation between Hβ luminosity and Fe

II EW (r=0.20) (here and in what follows, r is the linear correlation coefficient; the number of degrees of freedom is in each case near 290). This confirms Gaskell (1985) result that NLS1s have weak Hβ rather than strong Fe II. At very high densities ($N_e > 10^{10}$ cm^{-3}), the hydrogen lines become thermalized and their intensity drops considerably (Rees et al. 1989) which is a possible explanation of the decrease of the Hβ EW in NLS1s (Gaskell 1985).

3.3.2. Correlation between the strength of the Fe II and [O III] emissions

Goodrich (1989) noted that a defining characteristic of NLS1s is that the ratio R_{5007} of the [O III]λ5007 flux to the total Hβ flux is <3. In fact, when the first NLS1s were observed spectroscopically, the spectra were of relatively low resolution and the permitted and forbidden lines were believed to have the same width; these objects could therefore be mistaken for Seyfert 2s except for the presence in their spectra of strong Fe II emission, a strong blue continuum and a small λ5007/Hβ ratio due to the unrecognized presence of a broad Hβ component; as, in Seyfert 2s, this ratio is larger than 3, a smaller value was an indication of the presence of a broad Hβ component. But Osterbrock (1981) has divided the Seyfert 1s into five subgroups: S1.0, 1.2, 1.5, 1.8 and 1.9 on the basis of the appearance of the Balmer lines; a quantitative definition of these subgroups has been given by Winkler (1992) using the value of R_{5007}: for S1.0s, R_{5007} <0.2, for S1.2, 0.2<R_{5007} <0.5, for S1.5, 0.5<R_{5007} <3. The higher values of R_{5007} observed in S1.8 and S1.9 are believed to be due to partial extinction of the broad Hβ component. It follows that, for all S1s which do not suffer extinction, the condition R_{5007} <3 is fulfilled. We have measured on our spectra the parameter R_{5007} (given in Table 3); we have excluded for the computation of R_{5007} the contribution of the H II regions mentioned above. All objects have R_{5007} values lower than 0.8 except IC 3599 for which it exceeds 3.

Boroson & Green (1992), Grupe et al. (1999) and McIntosh et al. (1999) found that Fe II is strong in objects with weak [O III] lines and vice versa. Let us note however that while Grupe et al. and McIntosh et al. found an anticorrelation between R_{5007} and Fe II EW, Boroson & Green found a strong anticorrelation, not between the Fe II and [O III] EWs, but rather between the Fe II EW and the ratio of the peak height of the [O III]λ5007 line to that of Hβ which depends both on the value of R_{5007} and the width of Hβ; this correlation results from the anticorrelation between R_{4570} and the Hβ FWHM.

In Fig. 11, we have plotted R_{5007} *vs* R_{4570} and Fe II EW. There is a weak anticorrelation between Fe II EW and R_{5007}, but not between R_{4570} and R_{5007}. Therefore we do not confirm that Fe II is strong when the [O III] lines are weak.

Figure 12 shows the broad Hβ luminosity *vs* the broad Hβ and λ5007 EWs, and R_{5007}; the Hβ luminosities and λ5007 EWs are not correlated; the weak anticorrelation between Hβ luminosity and R_{5007} is due to the weakness of the Hβ EW in low luminosity objects, rather than to the strength of the λ5007 EW.

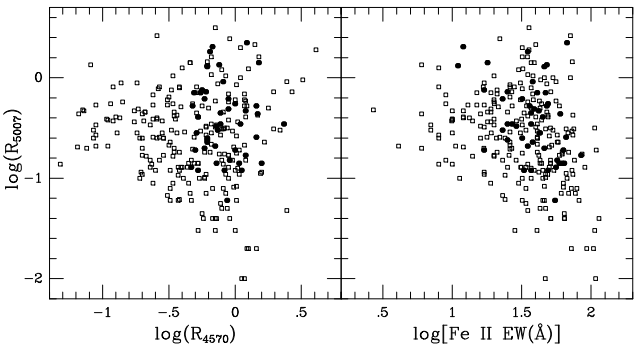

Fig. 11. Plot of R_{5007} *vs* R_{4570} (left panel) and Fe II EW (right panel) for several samples of Seyfert 1s. There is no correlation between R_{5007} and R_{4570} (r=0.05), while there is a trend for objects with a large Fe II EW to have a weak R_{5007} (r=0.29). The symbols are as in Fig. 10.

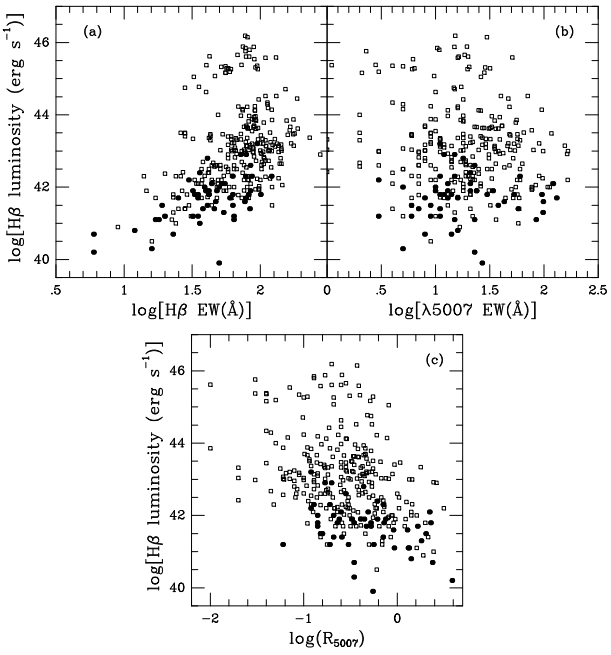

Fig. 12. Plots of the broad Hβ luminosity: in (a) *vs* the EW of the broad Hβ component (as in fig. 10); in (b), *vs* the λ5007 EW. It is a scatter diagram (r=0.16). As a result, the Hβ luminosity is anticorrelated with R_{5007} (r=0.43) (c). The symbols are as in Fig. 10.

3.4. On the definition of NLS1s

Initially, as we have seen, NLS1s were defined as having narrow "broad" Balmer components (<2 000 km s^{-1} FWHM). However, there is a continuous distribution of optical line widths in Seyfert 1s and the separation

between BLS1s and NLS1s is arbitrary (Turner et al. 1999b; Sulentic et al. 2000a). Sulentic et al. (2000a) suggested that Seyfert 1s with Hβ FWHM <4 000 km s^{-1} constitute a homogeneous class of objects having strikingly different line profiles compared to Seyfert 1s with broader lines. Grupe et al. (1999) have found objects displaying NLS1 properties (strong Fe II emission, a soft X-ray excess and variability) in spite of their Hβ FWHM exceeding 2 000 km s^{-1}. IRAS 10026+4347 has a large soft X-ray excess (Γ=3.2±0.5 or 2.9±0.2), strong Fe II emission (R_{4570}=2.0), and a high amplitude X-ray variability (×8); but the Hβ FWHM is ∼ 2 500 or 2 990 km s^{-1} (Grupe et al. 1998; Xia et al. 1999). Similarly, PDS 456 has a Hβ FWHM equal to 3 500 km s^{-1} although the Fe II lines are relatively strong (R_{4570}=0.46) (Simpson et al. 1999) and the X-ray spectrum shows a soft excess (Γ=3.9±0.8) (Reeves et al. 2000; Vignali et al. 2000). A few objects are known which have strong Fe II emission and relatively broad Hβ lines, but no soft X-ray excess; Mark 231 and IRAS 07598+6508 are two such examples. Mark 231 has a strong Fe II emission (R_{4570}=2.03 or 1.60), its Hβ FWHM is ∼ 3 000 km s^{-1} (Boroson & Meyers 1992; Lipari et al. 1993); the hard X-ray spectrum is heavily attenuated making it difficult to detect the eventual presence of a soft X-ray component (Turner 1999). IRAS 07598+6508 also has strong Fe II emission (R_{4570}=2.60) and a relatively broad Hβ line (2 550–3 200 km s^{-1} FWHM) (Lawrence et al. 1997; Lipari et al. 1993; Boroson & Meyers 1992); it is probably a highly obscured X-ray source (Gallagher et al. 1999).

We have plotted in Fig. 13, H$\beta_{\rm br}$ FWHM *vs* R_{4570} for all objects in our sample as well as in the other samples listed above; this plot shows a trend for the objects with the strongest Fe II emission to have narrower Balmer lines, with FWHM up to 3 500 km s^{-1}. We have drawn a line such that, for most objects below this line, R_{4570} >0.50 while, for many objects above it, R_{4570} < 0.50. This could be a better definition of NLS1s.

Figure 14 is a plot of the *ROSAT* photon index Γ *vs* R_{4570}; open circles represent the objects above the line in Fig. 13 and filled circles the objects below this line. This figure shows a definite correlation between Γ and R_{4570}. Although the objects with strong Fe II emission (black dots) show a large dispersion in Γ, most objects with small Fe II have Γ < 2.9.

Among the objects classified as NLS1s, having both narrow "broad" Balmer components and a strong Fe II emission, two have a very small photon index: IRAS 09571+8435 (Γ=1.39) and Mark 507 (Γ=1.68). Mark 507 has an intrinsic neutral hydrogen column density N_H=27×10^{20} cm^{-2} (see notes), this value being derived assuming that the intrinsic X-ray spectrum is a single power-law; it is quite possible that the column density is even higher and hides a soft X-ray component; this could also be true for IRAS 09571+8435.

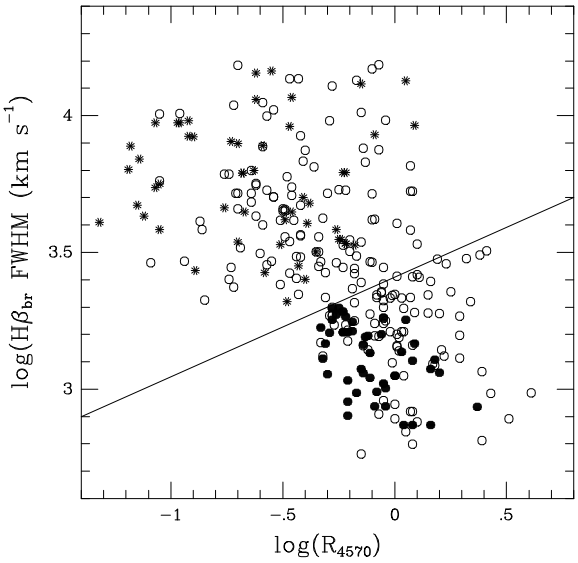

Fig. 13. Plot of the broad Hβ component FWHM *vs* R_{4570}. Filled circles represent the objects in our sample, open circles other radio quiet objects and stars radio loud objects; the correlation between the two parameters is strong (r=0.54). The straight line divides the plane into BLS1s (above the line) and what could be the newly defined class of NLS1s (below the line).

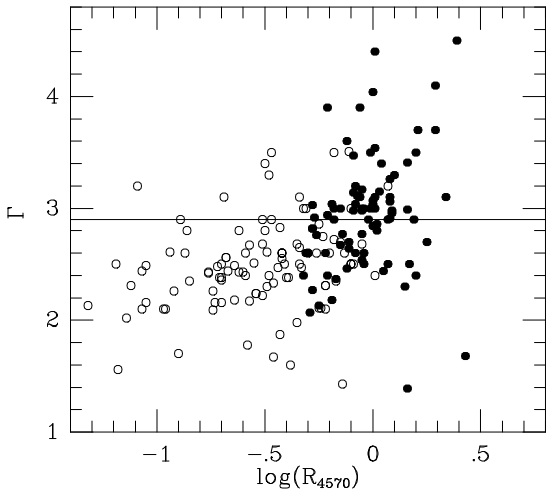

Fig. 14. Plot of the *ROSAT* photon index Γ *vs* R_{4570}. Filled circles represent the points below the line in the previous figure and open circles the points above the line. This diagram clearly shows that the soft X-ray excess tends to be large when the Fe II emission is large (r=0.40).

The FWHM of the broad Hβ component has been found to increase with the Hβ luminosity (Miller et al. 1992). Figure 15 is a plot of the Hβ luminosity *vs* the Hβ FWHM; the correlation between these two parameters is indeed quite strong; the linear correlation coefficient is r=0.76 for 294 data points, corresponding to a probability

p<0.01% for no correlation between the two parameters; luminous BLS1s tend to have broader Balmer lines (but we should keep in mind that the published Hβ FWHM have not been measured in a uniform way and that the presence of the narrow component of the line has not always been taken properly into account). This leads to question whether the defining criterion for NLS1s should be a function of luminosity (Wills et al. 2000).

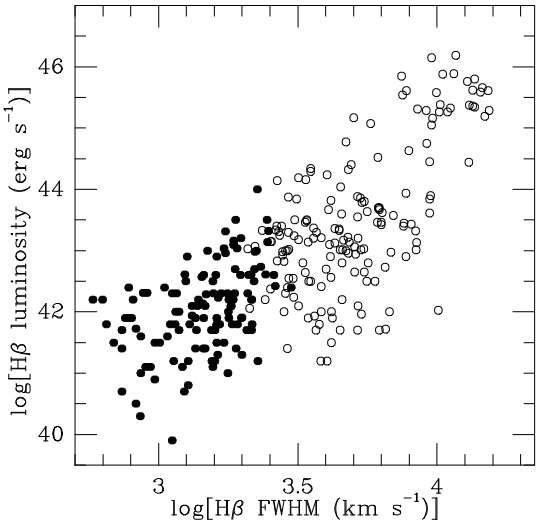

Fig. 15. Plot of the broad Hβ luminosity *vs* the FWHM of the broad Hβ component. The symbols are as in Fig. 14. There is clearly a strong correlation between the two plotted parameters (r=0.76).

4. Conclusions

In most cases, the broad Balmer components of NLS1s are well fitted by a single Lorentzian profile, confirming previous claims that Lorentzian rather than Gaussian profiles are better suited to reproduce the shape of the broad lines in NLS1s. This has consequences concerning their FWHMs and line ratios: when the broad Balmer components are fitted with a Lorentzian, most narrow line regions have line ratios typical of Seyfert 2s, while when they are fitted with a Gaussian they are widely scattered in the usual diagnostic diagrams; moreover, the FWHM of the best fitting Lorentzian is systematically smaller than the FWHM of the Gaussian. The Lorentzian shape of the broad emission lines could be the result of these lines being produced in a large disk.

We find that the [O III] lines usually have a relatively narrow Gaussian profile ($\sim$ 200–500 km s^{-1} FWHM) with often, in addition, a second broad ($\sim$ 500–1 800 km s^{-1} FWHM), blueshifted Gaussian component.

We do not confirm that the [O III] lines are weak in NLS1s.

As previously suggested, there is a continuous transition of all properties between NLS1s and BLS1s. The strength of Fe II relative to Hβ (R_{4570}) could be the best parameter to recognize an NLS1 defined as a Seyfert 1 with a high accretion rate. The maximum FWHM of the broad Balmer component of NLS1s could be an increasing function of the Hβ luminosity.

As all objects with Hβ FWHM smaller than 2 000 km s^{-1} seem to be genuine NLS1s, we plan to make similar spectroscopic observations of a sizeable sample of Seyfert 1s with 2 000 < Hβ FWHM < 4 000 km s^{-1} in the hope of better define the properties of those galaxies intermediate between NLS1s and BLS1s.

5. Notes on individual objects

Mark 335 (0003+19) is an NLS1 with strong Fe II emission and narrow "broad" Balmer lines (R_{4570}=0.62 and Hβ FWHM=1 640 km s^{-1}) (Boroson & Green 1992) and relatively strong coronal lines (Grandi 1978).

The broad Balmer components clearly have a complex and asymmetrical profile (van Groningen 1987; Arav et al. 1997); to get a satisfactory fit of our spectra, two broad components were necessary, a Gaussian and a Lorentzian.

I Zw 1 (0050+12) is the prototype NLS1; its optical spectrum reveals narrow emission lines and strong Fe II emission (Phillips 1976). The Hβ FWHM is in the range 1 050–1 500 km s^{-1} (Osterbrock 1977a; Phillips 1978a; Peterson et al. 1982; de Robertis 1985) although Wilkes et al. (1999) measured 2 590 km s^{-1}. The broad Balmer components clearly have a complex and asymmetrical profile; to get a satisfactory fit of our spectra, two Lorentzians were needed.

An UV spectrum shows that ions of increasing ionization level show increasing excess blue-wing flux and an increasing line peak velocity shift (Laor et al. 1997b). UV absorption lines have been observed, indicating the likely presence of a warm absorber (Crenshaw et al. 1999).

Ton S180 (0054−22) is an NLS1 (Comastri et al. 1998) with strong Fe II emission (R_{4570}=0.84, Comastri et al. 1998, or 1.02, Winkler 1992) and narrow Balmer lines (FWHM$\sim$1 000 km s^{-1}) (Winkler 1992; Comastri et al. 1998; Grupe et al. 1999).

Mark 359 (0124+18) is an NLS1 (Osterbrock & Pogge 1985). The FWHM of the broad Hα component is 780 km s^{-1}; the forbidden lines are exceptionally narrow (FWHM$\sim$100 km s^{-1}) (Veilleux 1991a). Discrepent values have been published for R_{4570} : 0.62 (Goodrich 1989) and <0.08 (Osterbrock & Pogge 1985). The coronal lines are very strong (Veilleux 1988; Erkens et al. 1997).

MS 01442−0055 (0144−00) is an NLS1 with Hβ FWHM= 1 940 km s^{-1} and R_{4570}=0.78 (Stephens 1989).

Mark 1044 (0227−09) is an NLS1 with strong narrow Fe II emission (Osterbrock & Dahari 1983). The Hβ FWHM is 1 280 (Goodrich 1989) or 1 400 km s^{-1} (Rafanelli 1985).

HS 0328+0528 (0328+05). The spectra published by Perlman et al. (1996) and Engels et al. (1998) suggest that it is an NLS1, although they do not show the presence of Fe II emission. Our spectra show that the broad Balmer components

are narrow ($\sim$ 1 500 km s^{-1}) which confirms the classification as an NLS1.

The [N II] lines are extremely weak; we measured λ6583/Hα= 0.12.

IRAS 03450+0055 (0345+00). Boroson & Meyers (1992) measured an Hα FWHM of 1 310 km s^{-1} and R_{4570}=0.96. Giannuzzo & Stirpe (1996) included it in their sample of NLS1s.

We have not observed this object.

IRAS 04312+4008 (0431+40) is an NLS1 with very strong Fe II emission: R_{4570}=2.36 (Moran et al. 1996). It is located at low galactic latitude: b=–5.0° with N_H $\sim$3.4$\times10^{21}$ cm^{-2}.

Mark 618 (0434−10). The Balmer line FWHM lies in the range 1 760–2 300 km s^{-1} (Osterbrock 1977a; Feldman & MacAlpine 1978; Phillips 1978a; Peterson et al. 1982; Boroson & Meyers 1992); it is a relatively strong Fe II emitter with R_{4570}=0.50 (Boroson & Meyers 1992). It has however been classified as a Seyfert 1 rather than an NLS1 by Moran et al. (1996).

It is a X-ray source, variable on a time scale of 1 000 s (Rao et al. 1992).

We have not observed this object.

IRAS 04416+1215 (0441+12) is an NLS1 with an Hβ FWHM =1 670 km s^{-1} (Moran et al. 1996). The [O III] lines are very broad (FWHM=1 150 km s^{-1} according to Moran et al. 1996); we find 1 320 km s^{-1}.

IRAS 04576+0912 (0457+09) is an NLS1 according to Moran et al. (1996) with Hβ FWHM=1 220 km s^{-1} and R_{4570}=1.51. It is a *ROSAT* X-ray source with a poorly determined photon index Γ=1.4±1.0 (Boller et al. 1992).

The [O III] lines are very broad (FWHM=1 310 km s^{-1} according to Moran et al. 1996; we find 1 290 km s^{-1}).

IRAS 04596−2257 (0459−22) is an NLS1 with Hβ FWHM $<$ 1 500 km s^{-1} (Green et al. 1989).

We have not observed this object.

IRAS 05262+4432 (0526+44) is an NLS1 with Hβ FWHM =700 km s^{-1} (Moran et al. 1996).

The narrow lines are clearly extended on our spectra, with λ6583/Hα $\sim$ 0.4 outside the nucleus; the 33 Å mm^{-1} red nuclear spectrum is well fitted by a Lorentzian (695 km s^{-1} FWHM) and two sets of narrow components with the same λ6583/Hα ratio $\sim$0.4 clearly coming from a H II region. The blue narrow line spectrum is composite: a H II region with weak [O III] emission and a Seyfert 2 nebulosity with weak Hβ which is too weak to be detected in either Hα nor [N II].

It is a *ROSAT* X-ray source with Γ=5.0, but the uncertainty in this value is large because of the high column density (Boller et al. 1992). It is located at a low galactic latitude: b=5.7°with N_H $\sim$ 3.8$\times10^{21}$ cm^{-2}.

RX J07527+2617 (0749+26) is an NLS1; the Balmer line FWHM is $\sim$ 1 000 km s^{-1} (Bade et al. 1995).

Mark 382 (0752+39) is an NLS1; the Hβ FWHM is 1 500 (Osterbrock 1977a) or 1 400 km s^{-1} (Peterson et al. 1982). We measured 1 280 km s^{-1}.

Mark 110 (0921+52) is a Seyfert 1 (Hutchings & Craven 1988). The Hβ FWHM is in the range 1 670–2 500 km s^{-1} (Osterbrock 1977a; Crenshaw 1986; Boroson & Green 1992; Bischoff & Kollatschny 1999). The Fe II emission is weak (R_{4570}=0.09–0.16) (Osterbrock 1977a; Meyers & Peterson 1985; Boroson & Green 1992); the Fe II line flux remains constant while the Balmer line fluxes vary (Bischoff & Kollatschny 1999).

We have not observed this object.

Mark 705 (0923+12). The Hβ FWHM is in the range 1 670–2 400 km s^{-1} (Zheng & O'Brien 1990; Miller et al. 1992; Boroson & Green 1992). We found that the broad Balmer components have a FWHM of $\sim$ 1 770 km s^{-1}. Coronal lines have been observed by Erkens et al. (1997).

Mark 707 (0934+01) is an NLS1; the Hβ FWHM is 1 320 (Boroson & Green 1992) or 2 000 km s^{-1} (Miller et al. 1992).

Mark 124 (0945+50) is an NLS1 (De Grijp et al. 1992); the FWHM of the broad Hβ component is in the range 1 050–1 400 km s^{-1} (Osterbrock 1977a; Phillips 1978a). Grandi (1978) did not find high excitation lines.

Mark 1239 (0949−01) is an NLS1 (Osterbrock & Pogge 1985); the FWHM of the broad Balmer components is $\sim$ 1 000 km s^{-1} (Osterbrock & Pogge 1985; de Robertis & Osterbrock 1984). In contrast, Rodríguez-Ardila et al. (2000b) gave 2 968 and 2 278 km s^{-1} FWHM for the broad Hβ and Hα component respectively but called it however an NLS1, while Rafanelli & Bonoli (1984) measured 5 000 and 4 800 km s^{-1} respectively. We have measured 1 075 and 905 km s^{-1} respectively, confirming that the object is an NLS1. Coronal lines have been observed by Rafanelli & Bonoli (1984) and Erkens et al. (1997).

IRAS 09571+8435 (0957+84) is an NLS1 with Hβ FWHM= 1 120 km s^{-1} and R_{4570}=1.46 (Moran et al. 1996).

Boller et al. (1992) found that the *ROSAT* photon index is Γ=1.39, a very small value for an NLS1, but the uncertainty is large.

PG 1011−040 (1011−04). The Hβ FWHM is 1 440 (Boroson & Green 1992) or 1 980 km s^{-1} (Miller et al. 1992). The spectrum published by Simpson et al. (1996) suggests that it is indeed an NLS1.

PG 1011−040 has been detected by *ASCA* as an X-ray source with a photon index Γ=1.93±0.41; its 2–10 keV luminosity is 6.3$\times10^{41}$ erg s^{-1}; it is a weak X-ray source for its optical luminosity (Gallagher et al. 2001).

PG 1016+336 (1016+33) is an NLS1 (Osterbrock & Pogge 1987). The Hβ FWHM is 1 310 km s^{-1} and R_{4570}=0.87 (Goodrich 1989).

Mark 142 (1022+51) is an NLS1; the Hβ FWHM is in the range 1 350–1 790 km s^{-1} (Osterbrock 1977a; Phillips 1978a; Boroson & Green 1992; Grupe et al. 1999).

KUG 1031+398 (1031+39). The broad component of the Balmer lines is relatively narrow and, consequently, this object has been classified as an NLS1 by Puchnarewicz et al. (1995).

The profile of the emission lines in KUG 1031+398 is complex; four emission components are present: an extended H II region, two distinct Seyfert-type clouds identified with the NLR (one of which has quite broad lines: ∼1 115 km s^{-1} FWHM), and a relatively narrow "broad line" component (1 060 km s^{-1} FWHM) (Gonçalves et al. 1999b).

According to Pounds et al. (1995), this object is unlike some other steep-spectrum (soft X-ray) AGNs in showing a marked absence of rapid X-ray variability and of strong Fe II line emission.

RX J10407+3300 (1037+33). The FWHM of the Balmer lines is 1 700 km s^{-1} and R_{4570}=0.56 (Bade et al. 1995) suggesting that it is an NLS1.

Mark 734 (1119+12). The spectrum published by Simpson et al. (1996) suggests that it is an NLS1; the Hβ FWHM is 1 820 (Boroson & Green 1992) or 1 940 km s^{-1} (Miller et al. 1992).

Mark 739E (1133+21). The double nucleus nature of Mark 739 was first described by Petrosian et al. (1979). The eastern component is an NLS1 with Hα FWHM=900 km s^{-1} and very strong Fe II emission (Netzer et al. 1987; Mazzarella & Boroson 1993). Our Lorentzian fit to the Balmer lines has a FWHM of ∼1 500 km s^{-1}, substantially larger than the published value.

MCG 06.26.012 (1136+34) is an NLS1; the Hβ FWHM is equal to 1 685 km s^{-1} (Grupe et al. 1999). Our observations confirm this classification.

Mark 42 (1151+46) is an NLS1 with relatively strong Fe II emission (Osterbrock & Pogge 1985). The Hβ emission line is very narrow, in the range 550–670 km s^{-1} FWHM (Osterbrock & Pogge 1985; Phillips 1978a). Grandi (1978) detected [Fe VII]λ6087.

On our spectra, the narrow lines are very narrow (< 200 km s^{-1} FWHM corrected for the instrumental broadening) and the line ratios are those of a H II region.

NGC 4051 (1200+44) is an NLS1 (Leighly 1999a). The Hβ FWHM is 990 (De Robertis & Osterbrock 1984) or 1 150 km s^{-1} (Leighly 1999b). The coronal lines are strong (Grandi 1978; Veilleux 1988; Erkens et al. 1997). Peterson et al. (2000) found that the Balmer lines could arise in a disk-like configuration and the high-ionization lines in an outflowing wind, of which we observe preferentially the near side. The structure and the kinematics of the [O III] lines also suggest an outflow (Christopoulou et al. 1997).

Our observations show the presence of two components in the [O III] lines, a narrow one (200 km s^{-1} FWHM) and a broader one (665 km s^{-1} FWHM) blueshifted by 175 km s^{-1} with respect to the first.

The X-ray source is variable by at least a factor 30 (Papadakis & Lawrence 1995; Leighly 1999a; Uttley et al. 1999; Komossa & Meerschweinchen 2000); long term variations in the average X-ray flux might in principle be caused by absorption by a varying column of material along the line of sight; but this is ruled out by the spectral data; it is the 2–10 keV luminosity which shows large amplitude long-term variations (Uttley et al. 1999).

PG 1211+143 (1211+14). The broad Balmer component FWHM has been measured to be in the range 1 500–1 860 (Zheng & O'Brien 1990; Stirpe 1990; 1991; Appenzeller & Wagner 1991; Miller et al. 1992; Boroson & Green 1992; Wilkes et al. 1999), except for Miller et al. (1992) who found 2 280 km s^{-1} for the FWHM of Hα. The [Fe VII] line was detected by Appenzeller & Wagner (1991).

The soft (0.1–2 keV) X-ray flux varied by at least a factor of 16 (Yaqoob et al. 1994).

Mark 766 (1215+30) is an NLS1 (Osterbrock & Pogge 1985). The Hβ FWHM is 1 600 (González Delgado & Pérez 1996) or 2 400 km s^{-1} (Osterbrock & Pogge 1985). Our own measurements give 1 150 and 1 630 km s^{-1} for the broad Hα and Hβ components respectively. The spectrum shows relatively strong Fe II emission (Meyers & Peterson 1985; González Delgado & Pérez 1996) and coronal lines (Veilleux 1988; González Delgado & Pérez 1996). The nucleus shows circumnuclear emission, the spectrum of which is well fitted by H II region models (González Delgado & Pérez 1996).

MS 12170+0700 (1216+07) has been identified with an AGN (Maccacaro et al. 1994). Our spectra show strong broad Balmer components with FWHM equal to 1 405 and 1 765 km s^{-1} for Hα and Hβ respectively; the narrow line system is most probably a H II region as shown by the line ratios (λ5007/Hβ=1.2 and λ6583/Hα=0.60).

MS 12235+2522 (1223+25) is an NLS1 with Hβ FWHM=1 730 km s^{-1} and λ5007 FWHM=1 700 km s^{-1} according to Stephens (1989). The broad Balmer components in our spectra were both fitted by a single Lorentzian (FWHM∼750 km s^{-1}).

IC 3599 (1235+26). An optical spectrum, taken in May 1991, shows permitted lines with widths ∼1 200–1 500 km s^{-1} showing that this object is an NLS1; the forbidden lines are narrow and weak ($R_{5007} < 0.1$) (Brandt et al. 1995; Mason et al. 1995). Low dispersion spectra taken by Grupe et al. (1995; 1999) from 1992 to 1995 show narrow Balmer and forbidden lines placing this object close to the borderline between Seyfert 2 and H II galaxies in the diagnostic diagrams of Veilleux & Osterbrock (1987); the resolution used was unsufficient to clearly show the composite nature of the spectrum; during this period, the line ratio R_{5007} was constant (3.3±0.3). Assuming that the [O III]λ5007 line flux is not variable, it follows that, between May 1991 and February 1992, the flux of the Balmer lines has decreased by a factor ∼27 (Grupe et al. 1995). [Fe VII] λ6087 have been detected (Komossa & Bade 1999).

Our spectra were taken in March 1997; the line ratio R_{5007} was then ∼3.3. The Hβ line was too weak for a significant fit to be made, but the broad Hα component could be fitted with a Lorentzian profile with a FWHM of ∼500 km s^{-1}.

IC 3599 has been detected as a *ROSAT* X-ray source (Bade et al. 1995). The 0.1–2.5 keV X-ray spectrum is extremely steep and is variable by an extremely large amount; the count-rate decreased by a factor of ∼80 from December 1990 to June 1992 and then by an additional factor of ∼2 to June 1993 (Grupe et al. 1995; Brandt et al. 1995; Mason et al. 1995).

PG 1244+026 (1244+02) is an NLS1; the FWHM of the Hβ line is 830 (Boroson & Green 1992) or 1 350 km s^{-1}

(Miller et al. 1992).

NGC 4748 (1249−13) is an NLS1 with strong Fe II emission (Osterbrock & de Robertis 1985; Moran et al. 1996). The Hβ FWHM is in the range 1 100–1 500 km s^{-1} (Osterbrock & de Robertis 1985; Maza & Ruiz 1989; Winkler 1992). Rodríguez-Ardila et al. (2000b) measured ∼2 350 km s^{-1} for the FWHM of the broad Balmer components. Our own measurements show that they have a FWHM of ∼1 500 km s^{-1}.

Mark 783 (1300+16) is an NLS1, however the Fe II emission is very weak: R_{4570} <0.11 (Osterbrock & Pogge 1985).

R 14.01 (1338−14) is an NLS1 with Hβ FWHM=1 790 km s^{-1} (Maza & Ruiz 1989).

Mark 69 (1343+29). Osterbrock (1977a) noted that it is a Seyfert 1 with relatively narrow "broad" Balmer lines (∼1 500 km s^{-1} FWHM). The emission lines on our spectra are well fitted with a single Lorentzian for the broad Balmer component and one set of Gaussians for the narrow lines, with line ratios indicating a H II region (λ5007/Hβ=2.23 and λ6583/Hα=0.67).

2E 1346+2646 (1346+26) is a Seyfert 1 with a relatively narrow "broad" Hβ component (Hill & Oegerle 1993). Our red spectrum is equally well fitted with either a broad Gaussian (FWHM=1680 km s^{-1}) or a broad Lorentzian (FWHM=1235 km s^{-1}). On the blue spectrum, the broad Hβ component is weak and the measurement quite uncertain.

PG 1404+226 (1404+22) is an NLS1 with a narrow Hβ line: 880 (Boroson & Green 1992) or 1 290 km s^{-1} FWHM (Miller et al. 1992).

The X-ray flux has changed by a factor 13.1 in 10 years (Forster & Halpern 1996) and by a factor 4 in ∼3×10^4 s (Ulrich et al. 1999).

Mark 684 (1428+28) is an NLS1 (Osterbrock & Pogge 1987) with prominent Fe II emission (Persson 1988).

On the red spectrum, the broad line component is poorly fitted by a single Lorentzian; a second, Gaussian component is needed. The broad Hβ line is too weak for a meaningful fit to be made. The spectrum is composite in the sense that the narrow line region has two components, one with relatively broad lines, the other with very narrow lines and line ratios typical of a H II region.

Mark 478 (1440+35) is an NLS1 (Gondhalekar et al. 1994; Moran et al. 1996). The Hβ FWHM is in the range 1 300–1 915 km s^{-1} (Phillips 1978a; Peterson et al. 1982; Boroson & Green 1992; Gondhalekar et al. 1994; Grupe et al. 1999). The Fe II emission is strong (Phillips 1977). Grandi (1978) could not detect high excitation lines.

PG 1448+273 (1448+27) is an NLS1; the Hβ FWHM is in the range 910–1 200 km s^{-1} (Stirpe 1991; Boroson & Green 1992).

IRAS 15091−2107 (1509−21) is an NLS1 (Osterbrock & de Robertis 1985), although Moran et al. (1996) rather classified it as a Seyfert 1. Goodrich (1989) measured Hβ FWHM= 1 480 km s^{-1} and R_{4570}= 0.54. Winkler (1992) and Maza & Ruiz (1989) measured 2 000 and 1 600 km s^{-1} respectively for the Hβ FWHM.

We have not observed this object.

MS 15198−0633 (1519−06) is an AGN (Margon et al. 1985). The Hβ FWHM is equal to 1 304 km s^{-1}; the [Fe VII]λ6087 line was not detected (Appenzeller & Wagner 1991). We have only a red spectrum with a relatively poor signal-to-noise ratio.

Mark 486 (1535+54). The Hβ FWHM is in the range 1 410–1 650 km s^{-1} (Boroson & Green 1992; de Robertis 1985; Osterbrock & Shuder 1982; Boroson et al. 1985). The Fe II emission is relatively strong (Phillips 1978a). Erkens et al. (1997) have observed coronal lines.

The X-ray source has an *ASCA* photon index Γ=2.02 ±0.93 and a high neutral absorption column density (N_H=1.2× 10^{23} cm^{-2} plus an unabsorbed component scattered by electrons towards the observer; its 2–10 keV luminosity is 1.3×10^{42} erg s^{-1}; if the optical nucleus was also absorbed by such a large column density, it would not be observable and the galaxy would appear as a Seyfert 2 (Gallagher et al. 2001).

IRAS 15462−0450 (1546−04) has been identified with the northern 16.6 mag spiral member of a loose interacting pair (Strauss et al. 1992; Duc et al. 1997). It is an ultraluminous IR galaxy with a Seyfert 1 spectrum and strong Fe II lines (Duc et al. 1997); the [O III] lines are broad with FWHM=1 560 km s^{-1} (Kim et al. 1998).

On our spectra, the broad Balmer components have a FWHM of ∼1 700 km s^{-1}; the narrow lines have a complex profile and can be fitted with two Gaussian systems: one has very narrow lines (<180 km s^{-1} FWHM corrected for instrumental broadening), with line ratios indicating that it is a H II region; the second system has very broad lines (∼ 1 600 km s^{-1} FWHM) and correspond to a Seyfert 2 nebulosity.

Mark 493 (1557+35) is an NLS1 with Hβ FWHM = 410 km s^{-1} (Osterbrock & Pogge 1985).

EXO 16524+3930 (1652+39) is an NLS1 with Balmer line FWHMs equal to 1 000 km s^{-1} (Bassani et al. 1989), which is confirmed by our own observations.

B3 1702+457 (1702+45) is an NLS1 according to Moran et al. (1996) and Wisotzki & Bade (1997) who give 490 and 800 km s^{-1} respectively for the Hβ FWHM. Leighly (1999b) measured R_{4570}=1.86.

Komossa & Bade (1998) have shown the presence of a warm absorber. The *ASCA* spectrum is well fitted by a single power law (Γ=2.20±0.06) plus Galactic absorption, a warm absorber and no soft excess (Leighly 1999b; Vaughan et al. 1999a).

RX J17450+4802 (1743+48) is a Seyfert 1 (Perlman et al. 1996). The Balmer line FWHM is 1 600 km s^{-1} (Bade et al. 1995). Our blue spectrum shows that the Hβ broad component FWHM is 1 355 km s $^{-1}$ and R_{4570}=0.78, so this object is an NLS1.

Kaz 163 (1747+68) is the southern member of an interacting pair. It is an NLS1 (Stephens 1989). The Hβ FWHM is in the range 1 040–2 110 km s^{-1} (Kriss & Canizares

1982; Stephens 1989; Goodrich 1989; Leighly 1999b).

Mark 507 (1748+68) has been variously classified as a HII region (Terlevich et al. 1991), a Seyfert 2 (Koski 1978) or a Liner with a "transition" type nucleus (Heckman 1980). It is however an NLS1 according to Halpern & Oke (1987), Goodrich (1989), Moran et al. (1996) and Leighly (1999b). The Hβ FWHM is 965 (Goodrich 1989) or 1 150 km s^{-1} (Leighly 1999b). The Fe II emission is strong with R_{4570}=2.71 (Goodrich 1989) or 1.45 (Leighly 1999b).

Our spectra show narrow "broad" Balmer components ($\sim$1 335 km s^{-1} FWHM). The [O III] lines and the narrow component of Hβ are best fitted by two sets of Gaussians, one with narrow components and weak [O III] lines, typical of a H II region, the other with much broader lines and a large λ5007/Hβ ratio. The presence of the H II region component is not very surprising as Halpern & Oke (1987) have found that the emission lines away from the nucleus are similar to those of a H II region.

The *ROSAT* photon index is Γ=1.68$\pm$0.16 (Leighly 1999b), with an intrinsic neutral hydrogen column density: N_H=27$\times$10^{20} cm^{-2} in excess of the Galactic value (Iwasawa et al. 1998; Leighly 1999b). The photon index of this object is very small for an NLS1; this could be due to the presence of a high column density.

HS 1817+5342 (1817+53). A spectrum published by Engels et al. (1998) suggests that this object could be an NLS1. Our spectra show that the broad Balmer line component FWHM are $\sim$1 620 km s^{-1} and R_{4570}=0.59, so there is no doubt that this is an NLS1.

HS 1831+5338 (1831+53). A spectrum published by Engels et al. (1998) suggests that this object could be an NLS1. Our spectra show that the FWHMs of the broad Balmer components are $\sim$1 510 km s^{-1} and R_{4570}=0.74, so there is no doubt that this is an NLS1.

Mark 896 (2043−02) is a Seyfert 1 with relatively narrow Balmer lines and strong Fe II emission (Osterbrock & Dahari 1983; Morris & Ward 1988). The Hβ FWHM is 1 390 (Stirpe 1991) or 1 330 km s^{-1} (Stirpe 1990). However Moran et al. (1996) classified it as a Seyfert 1 rather than an NLS1. Our spectra show quite narrow "broad" Balmer components ($\sim$1 100 km s^{-1}) and R_{4570}=0.50, so it is an NLS1.

MS 22102+1827 (2210+18) has been identified with an AGN (Stocke et al. 1991; Maccacaro et al. 1994). Our spectra show quite narrow "broad" Balmer components ($\sim$ 750 km s^{-1}), so this is most probably an NLS1.

Akn 564 (2240+29) is an NLS1 (Goodrich 1989). The Hα and Hβ FWHM lie in the ranges 600–730 and 720–1 030 km s^{-1} respectively (Osterbrock & Shuder 1982; de Robertis & Osterbrock 1984; Stirpe 1990; 1991; Moran et al. 1996; Comastri et al. 2001). The coronal lines are strong (Veilleux 1988; Erkens et al. 1997; Comastri et al. 2001).

The X-ray flux varies by $\sim$50% in 1.6 h; the X-ray light-curve shows no evidence for energy dependence of the variability within the 0.6–10 keV bandpass (Turner et al. 1999a; Vaughan et al. 1999b).

UV absorption lines have been detected, indicating the presence of a warm absorber (Crenshaw et al. 1999).

HS 2247+1044 (2247+10). A spectrum published by Engels et al. (1998) suggested that this object could be an NLS1. This classification is confirmed by our spectra.

Kaz 320 (2257+24) is an NLS1 according to Zamorano et al. (1992) who measured 1 700 and 1 800 km s^{-1} for the FWHM of the broad component of Hα and Hβ respectively. Our spectra confirm this classification.

Acknowledgements. We thank C. Boisson for a careful reading of the manuscript.

References

Aoki K., Yoshida M. 1999,ASP Conf. Ser. 162,385
Appenzeller I., Wagner S.J. 1991,A&A 250,57
Arav N., Barlow T.A., Laor A., Blandford R.D. 1997,MNRAS 288,1015
Arribas S., Mediavilla E. 1993,ApJ 410,552
Bade N., Fink H.H., Engels D. et al. 1995,A&AS 110,469
Bassani L., Coe M.J., Malkan M.A. et al. 1989,ApJ 344,726
Bergeron J., Kunth D. 1984,MNRAS 207,263
Bischoff K., Kollatschny W. 1999,A&A 345,49
Boller T., Meurs E.J.A., Brinkmann W. et al. 1992,A&A 261,57
Boller T., Brandt W.N., Fink H. 1996,A&A 305,53
Boroson T.A., Green R.F. 1992,ApJS 80,109
Boroson T.A., Meyers K.A. 1992,ApJ 397,442
Boroson T.A., Persson S.E., Oke J.B. 1985,ApJ 293,120
Bottorff M., Korista K.T., Schlosman I., Blandford R.D. 1997,ApJ 479,200
Brandt W.N., Pounds K.A., Fink H. 1995,MNRAS 273,L47
Brandt W.N., Mathur S., Elvis M. 1997,MNRAS 285,L25
Brandt W.N., Boller T., Fabian A.C., Ruszkowski M. 1999,MNRAS 303,L53
Brotherton M.S. 1996,ApJS 102,1
Brotherton M.S., Wills B.J., Francis P.J., Steidel C.C. 1994,ApJ 430,495
Christopoulou P.E., Holloway A.J., Steffen W. et al. 1997,MNRAS 284,385
Ciliegi P., Maccacaro T. 1996,MNRAS 282,477
Clavel J., Joly M., Collin-Souffrin S., Bergeron J., Penston M.V. 1983, MNRAS 202,85
Colbert E.J.M., Baum S.A., Gallimore J.F. et al. 1996,ApJS 105,75
Collin-Souffrin S., Lasota J.-P. 1988,PASP 100,1041
Collin-Souffrin S., Dumont S., Heidmann N., Joly M. 1980,A&A 83,190
Collin-Souffrin S., Dyson J.E., McDowell J.C., Perry J.J. 1988a,MNRAS 232,539
Collin-Souffrin S., Hameury J.-M., Joly M. 1988b,A&A 205,19
Comastri A., Fiore F., Guainazzi M. et al. 1998,A&A 333,31
Comastri A., Stirpe G.M., Vignali C. et al. 2001,A&A 365,400
Corbin M.R. 1995,ApJ 447,496
Corbin M.R. 1997,ApJS 113,245
Corbin M.R., Boroson T.A. 1996,ApJS 107,69
Crenshaw D.M. 1986,ApJS 62,821
Crenshaw D.M., Kraemer S.B. 2000,ApJ 532,L101
Crenshaw D.M., Kraemer S.B., Boggess A. et al. 1999,ApJ 516,750

Crenshaw D.M., Kraemer S.B., Hutchings J.B. et al. 2000,AJ 120,1731
de Grijp M.H.K., Keel W.C., Miley G.K., Goudfrooij P., Lub J. 1992,A&AS 96,389
de Robertis M.M. 1985,ApJ 289,67
de Robertis M.M., Osterbrock D.E. 1984,ApJ 286,171
Duc P.A., Mirabel I.F., Maza J. 1997,A&AS 124,533
Dumont A.-M., Collin-Souffrin S. 1990,A&A 229,313
Dumont A.-M., Collin-Souffrin S., Nazarova L. 1998,A&A 331,11
Elvis M., Green R.F., Bectold J., Fabbiano G. 1986,ApJ 310,291
Emmering R.T., Blandford R.D., Shlosman I. 1992,ApJ 385,460
Engels D., Hagen H.-J., Cordis L. et al. 1998,A&AS 128,507
Erkens U., Appenzeller J., Wagner S. 1997,A&A 323,707
Feldman F.R., MacAlpine G.M. 1978,ApJ 221,486
Fiore F., Laor A., Elvis M., Nicastro F., Giallongo E. 1998,ApJ 503,607
Forster K., Halpern J.P. 1996,ApJ 468,565
Francis P.J., Hewett P.C., Foltz C.B., Chaffee F.H. 1992,ApJ 398,476
Gallagher S.C., Brandt W.N., Sambruna R.M. et al. 1999,ApJ 519,549
Gallagher S.C., Brandt W.N., Laor A. et al. 2001,ApJ 546,795
Gaskell C.M. 1985,ApJ 291,112
Gaskell C.M. 2000,New Astronomy Review 44,563
George I.M., Turner T.J., Netzer H. et al. 1998a,ApJS 114,73
George I.M., Mushotzky R., Turner T.J. et al. 1998b,ApJ 509,146
George I.M., Turner T.J., Yaqoob T. et al. 2000,ApJ 531,52
Giannuzzo M.E., Stirpe G.M. 1996,A&A 314,419
Gliozzi M., Boller T., Brinkmann W., Brandt W.N. 2000,A&A 356,L17
Goad M.R., Koratkar A.P., Kim-Quijano J. et al. 1999,ApJ 524,707
Gonçalves A.C., Véron P., Véron-Cetty M.-P. 1999a,A&AS 135,437
Gonçalves A.C., Véron P., Véron-Cetty M.-P. 1999b,A&A 341,662
Gondhalekar P.M., Kellett B.J., Pounds K.A., Matthews L., Quenby J.J. 1994, MNRAS 268,973
González Delgado R.M., Pérez E. 1996,MNRAS 278,737
Goodrich R.W. 1989,ApJ 342,224
Grandi S.A. 1978,ApJ 221,501
Green P.J., Ward M.J., Anderson S.F. et al. 1989,ApJ 339,93
Grupe D., Beuerman K., Mannheim K. et al. 1995,A&A 299,L5
Grupe D., Beuerman K., Thomas H.C. et al. 1998,A&A 330,25
Grupe D., Beuerman K., Mannheim K., Thomas H.C. 1999,A&A 350,805
Halpern J.P., Oke J.B. 1987,ApJ 312,91 of IPC X-ray sources, Smithsonian astrophysical observatory, Cambridge
Heckman T.M. 1980,A&A 87,152
Heckman T.M., Miley G.K., van Breugel W.J.M., Butcher H.R. 1981,ApJ 247,403
Heckman T.M., Miley G.K., Green R.F. 1984,ApJ 281,525
Hill J.M., Oegerle W.R. 1993,AJ 106,831
Hutchings J.B., Craven S.E. 1988,AJ 95,677
Iwasawa K., Brandt W.N., Fabian A.C. 1998,MNRAS 293,251
Joly M. 1981,A&A 102,321
Kaiser M.E., Bradley L.D., Hutchings J.B. et al. 2000,ApJ 528,260
Kim D.-C., Veilleux S., Sanders D.B. 1998,ApJ 508,627
Kolman M., Halpern J.P., Shrader C.R. et al. 1993,ApJ 402,514
Komossa S., Fink H. 1997a,A&A 327,483
Komossa S., Fink H. 1997b,A&A 327,555
Komossa S., Bade N. 1998,A&A 331,L49
Komossa S., Bade N. 1999,A&A 343,775
Komossa S., Meerschweinchen J. 2000,A&A 354,411
Königl A., Kartje J.F. 1994,ApJ 434,446
Koski A.T. 1978,ApJ 223,56
Kriss G.A., Canizares C.R. 1982,ApJ 261,51
Kuraszkiewicz J.K., Wilkes B.J., Czerny B., Mathur S. 2000,ApJ 542,692
Kwan J., Cheng F.-Z., Fang L.-Z., Zheng W., Ge J. 1995,ApJ 440,628
Laor A., Fiore F., Elvis M., Wilkes B.J., McDonnel J.C. 1997a,ApJ 477,93
Laor A., Jannuzi B.T., Green R.F., Boroson T.A. 1997b,ApJ 489,656
Lawrence A., Saunders W., Rowan-Robinson M. et al. 1988,MNRAS 235,261
Lawrence A., Elvis M., Wilkes B.J., McHardy I., Brandt N. 1997,MNRAS 285,879
Leighly K.M. 1999a,ApJS 125,297
Leighly K.M. 1999b,ApJS 125,317
Leighly K.M. 2001,ASP Conf. Ser. 224, HST SIS ultraviolet spectral evidence for outflows in extreme narrow-line Seyfert 1 galaxies, B.M. Peterson, R.S. Polidan, R.W. Pogge eds. (in press)
Lemaître G., Kohler D., Lacroix D., Meunier J.-P., Vin A. 1989,A&A 228,546
Lipari S. 1994,ApJ 436,102
Lipari S., Terlevich R., Macchetto F. 1993,ApJ 406,451
Maccacaro T., Wolter A., McLean B. et al. 1994,Astrophys. Lett. & Comm. 29,267
Margon B., Downes R.A., Chanan G.A. 1985,ApJS 59,23
Marziani P., Sulentic J.W., Dultzin-Hacyan D., Calvani M., Moles M. 1996,ApJS 104,37
Mason K.O., Hassall B.J.M., Bromage G.E. et al. 1995,MNRAS 274,1194
Massey P., Strobel K., Barnes J.V., Anderson E. 1988,ApJ 328,315
Mathews W.G., Wampler E.J. 1985,PASP 97,966
Maza J., Ruiz M.T. 1989,ApJS 69,353
Mazzarella J.M., Boroson T.A. 1993,ApJS 85,27
McIntosh D.H., Rieke M.J., Rix H.-W., Foltz C.B., Weyman R.J. 1999,ApJ 514,40
Meyers K.A., Peterson B.M. 1985,PASP 97,734
Miller P., Rawlings S., Saunders R., Eales S. 1992,MNRAS 254,93
Molthagen K., Bade N., Wendker H.J. 1998,A&A 331,925
Moran E.C., Halpern J.P., Helfand D.J. 1996,ApJS 106,341
Morris S.L., Ward M.J. 1988,MNRAS 230,639
Murray N., Chiang J. 1998,ApJ 494,125
Nagao T., Murayama T., Taniguchi Y. 2001,ApJ 546,744
Nandra K., Pounds K.A. 1994,MNRAS 268,405
Netzer H., Kollatschny W., Fricke K.J. 1987,A&A 171,41
Nicastro F. 2000,ApJ 530,L65
Oke J.B. 1974,ApJS 27,21
Oke J.B., Gunn J.E. 1983,ApJ 206,713
Osterbrock D.E. 1977a,ApJ 215,733
Osterbrock D.E. 1977b,PASP 89,620
Osterbrock D.E. 1981,ApJ 249,462
Osterbrock D.E. 1987,Lecture notes in Physics 307,1
Osterbrock D.E., Dahari O. 1983,ApJ 273,478

Osterbrock D.E., Shuder J.M. 1982,ApJS 49,149
Osterbrock D.E., de Robertis M.M. 1985,PASP 97,1129
Osterbrock D.E., Pogge R.W. 1985,ApJ 297,166
Osterbrock D.E., Pogge R.W. 1987,ApJ 323,108
Page M.J., Carrera F.J., Mittaz J.P.D., Mason K.O. 1999,MNRAS 305,775
Papadakis I.E., Lawrence A. 1995,MNRAS 272,161
Perlman E.S., Stocke J.T., Schachter J.F. et al. 1996,ApJS 104,251
Persson S.E. 1988,ApJ 330,751
Peterson B.M., Foltz C.G., Byard P.L., Wagner R.M. 1982,ApJS 49,469
Peterson B.M., Pogge R.W., Wanders I. 1999,ASP Conf. Ser. 175,41
Peterson B.M., McHardy I.M., Wilkes B.J. et al. 2000,ApJ 542,161
Petrosian A.R., Saakian K.A., Khachikian E.E. 1979,Astrophys. 15,250
Pfefferkorn F., Boller T., Rafanelli P. 2001,A&A 368,797
Phillips M.M. 1976,ApJ 208,37
Phillips M.M. 1977,ApJ 215,746
Phillips M.M. 1978a,ApJS 38,187
Phillips M.M. 1978b,ApJ 226,736
Pogge R.W. 1989,ApJ 345,730
Pounds K.A., Stanger V.J., Turner T.J., King A.R., Czerny B. 1987,MNRAS 224,443
Pounds K.A., Done C., Osborne J.P. 1995,MNRAS 277,L5
Puchnarewicz E.M., Mason K.O., Córdova F.A. et al. 1992,MNRAS 256,589
Puchnarewicz E.M., Mason K.O., Córdova F.A. et al. 1994,MNRAS 270,663
Puchnarewicz E.M., Mason K.O., Siemiginowska A., Pounds K. 1995,MNRAS 276,20
Puchnarewicz E.M., Mason K.O., Carrera F.J. et al. 1997,MNRAS 291,177
Rafanelli P. 1985,A&A 146,17
Rafanelli P., Bonoli C. 1984,A&A 131,186
Rao A.R., Singh K.P., Vahia M.N. 1992,MNRAS 255,197
Rees M.J., Netzer H., Ferland G.J. 1989,ApJ 347,640
Reeves J., Turner M.J.L. 2000,MNRAS 316,234
Reeves J., O'Brien P.T., Vaughan S. et al. 2000,MNRAS 312,L17
Reynolds C.S. 1997,MNRAS 286,513
Rodríguez-Ardila A., Pastoriza M.G., Donzelli C.J. 2000a,ApJS 126,63
Rodríguez-Ardila A., Binette L., Pastoriza M.G., Donzelli C.J. 2000b,ApJ 538,581
Rodríguez-Pascual P.M., Mas-Hesse J.M., Santos-Lléo M. 1997,A&A 327,72
Ross R.R., Fabian A.C., Mineshige S. 1992,MNRAS 258,189
Rush B., Malkan M.A., Fink H.H., Voges W. 1996,ApJ 471,190
Sanders D.B., Phinney E.S., Neugebauer G., Soifer B.T., Matthews K. 1989,ApJ 347,29
Saxton R.D., Turner M.J.L., Williams O.R. et al. 1993,MNRAS 262,63
Siemiginowska A., Kuhn O., Elvis M. et al. 1995,ApJ 454,77
Simpson C., Ward M., Clements D.L., Rawlings S. 1996,MNRAS 281,509
Simpson C., Ward M., O'Brien P., Reeves J. 1999,MNRAS 303,L23
Smith S.J. 1993,ApJ 411,570
Stephens S.A. 1989,AJ 97,10
Stirpe G.M. 1990,A&AS 85,1049
Stirpe G.M. 1991,A&A 247,3
Stocke J.T., Morris S.L., Gioia I.M. et al. 1991,ApJS 76,813
Stone R.P.S. 1977,ApJ 218,767
Storchi-Bergmann T., Wilson A.S., Baldwin J.A. 1992,ApJ 396,45
Strauss M.A., Huchra J.P., Davis M. et al. 1992,ApJS 83,29
Sulentic J.W., Marziani P., Dultzin-Hacyan D., Calvani M., Moles M. 1995, ApJ 445,L85
Sulentic J.W., Zwitter T., Marziani P., Dultzin-Hacyan D. 2000a,ApJ 536,L5
Sulentic J.W., Marziani P., Zwitter T., Dultzin-Hacyan D., Calvani M. 2000b, ApJ 545,L15
Sun W.-H., Malkan M.A. 1989,ApJ 346,68
Terlevich R., Melnick J., Masegosa J., Moles M., Copetti M.V.F. 1991,A&AS 91,285
Turner T.J. 1999,ApJ 511,142
Turner T.J., George I.M., Netzer H. 1999a,ApJ 526,52
Turner T.J., George I.M., Nandra K., Turcan D. 1999b,ApJ 524,667
Ulrich-Demoulin M.-H., Molendi S. 1996,ApJ 457,77
Uttley P., M^{c}Hardy I.M., Papadakis I.E., Guainazzi M., Fruscione A. 1999,MNRAS 307,L6
van Groningen E. 1987,A&A 186,103
Vaughan S., Reeves J., Warwick R., Edelson R. 1999a,MNRAS 309,113
Vaughan S., Pounds K.A., Reeves J., Warwick R., Edelson R. 1999b,MNRAS 308,L34
Veilleux S. 1988,AJ 95,1695
Veilleux S. 1991a,ApJ 368,158
Veilleux S. 1991b,ApJS 75,383
Veilleux S., Osterbrock D.E. 1987,ApJS 63,295
Veilleux S., Shopbell P.L., Miller S.T. 2001,AJ 121,198
Véron P., Véron-Cetty M.P. 1986, A&A 161,145
Véron P., Lindblad P.O., Zuiderwijk E.J., Véron-Cetty M.P., Adam G. 1980, A&A 87,245
Véron P., Véron-Cetty M.P., Zuiderwijk E.J. 1981a, A&A 102,116
Véron P., Véron-Cetty M.P., Bergeron J., Zuiderwijk E.J. 1981b, A&A 97,71
Véron M.-P. 1981,A&A 100,12
Véron-Cetty M.-P., Véron P., Gonçalves A.C. 2001,in preparation
Vignali C., Comastri A., Nicastro F. et al. 2000,A&A 362,69
Vrtilek J.M. 1985,ApJ 294,121
Vrtilek J.M., Carleton N.P. 1985,ApJ 294,106
Walter R., Fink H.H. 1993,A&A 274,105
Wang T., Brinkmann W., Bergeron J. 1996,A&A 309,81
Wang T.-G., Lu Y.-J., Zhou Y.-Y. 1998,ApJ 493,1
Whittle M. 1985a,MNRAS 213,1
Whittle M. 1985b,MNRAS 213,33
Whittle M. 1992,ApJ 387,109
Whittle M., Pedlar A., Meurs E.J.A. et al. 1988,ApJ 326,125
Wilkes B.J., Kuraszkiewicz J., Green P.J., Mathur S., McDonnel J.C. 1999,ApJ 513,76
Wills B.J. 1982,IAU Symp. 97,373
Wills B.J., Brotherton M.S., Fang D., Steidel C.C., Sargent W.L.W. 1993,ApJ 415,563
Wills B.J., Laor A., Brotherton M.S. et al. 1999,ApJ 515,L53
Wills B.J., Shang Z., Yuan J.M. 2000,New Astronomy Review 44,511
Wilson A.S. 1994,in: Oxford astrophysics workshop on "Evidence for the torus", ed. M.J. Ward, p. 55
Wilson A.S., Braatz J.A., Heckman T.M., Krolik J.H., Miley G.K. 1993,ApJ 419,L61

Winkler H. 1992,MNRAS 257,677
Wisotzki L., Bade N. 1997,A&A 320,395
Wisotzki L., Dreizler S., Engels D., Fink H.-H., Heber U. 1995,A&A 297,L55
Xia X.-Y., Mao S., Wu H. et al. 1999,A&A 341,L13
Yaqoob T., Serlemitsos P., Mushotzky R. et al. 1994,PASJ 46,L173
Yuan W., Brinkmann W., Siebert J., Voges W. 1998,A&A 330,108
Zamorano J., Gallego J., Rego M., Vitores A.G., Gonzalez-Riesta R. 1992,AJ 104,1000
Zheng W., O'Brien P.T. 1990,ApJ 353,433
Zheng W., Keel W.C. 1991,ApJ 382,121